Genesis of the Singhbhum craton, eastern India; implications for Archean crust-mantle evolution of the Earth

Om Prakash Pandey[1]*, Klaus Mezger[1], Dewashish Upadhyay[2], Sameer Ranjan[2], Igor M. Villa[1,3], Thomas F. Nägler[1], Hauke Vollstaedt[1, +4]

[1]Institute of Geological Sciences, University of Bern, Baltzerstrasse 1+3, 3012 Bern, Switzerland

[2]Department of Geology and Geophysics, Indian Institute of Technology, Kharagpur, India

[3]Centro Universitario Datazioni e Archeometria, Universita`di Milano Bicocca, Piazza della Scienza 4, 20126 Milano, Italy

[+]Present address: [4]Thermo Fisher Scientific, Hanna-Kunath-Str. 11, 28199 Bremen, Germany

*Corresponding author: Om Prakash Pandey

Address: Institute of Geological Sciences, University of Bern, Baltzerstrasse 1+3, 3012 Bern, Switzerland.

E-mail: om.pandey@geo.unibe.ch

Phone: +41-31-631-4016

Abstract

The Singhbhum craton in eastern India, one of the four major Archean cratons of Indian Shield, is ~~mainly~~ underlain by Paleoarchean granitoids (trondhjemite-tonalite-granodiorite i.e. TTGs, and potassic granites) that are encircled by greenstone belts rich in banded iron formation known as Iron Ore Group. This study presents whole rock major-trace elements, Sr and Nd isotopes, K-feldspar common Pb isotopes, along with in-situ zircon U-Pb age and Hf isotopes data to characterize the source(s) of these rocks and their role in evolution of the Paleoarchean continental crust. Zircon U-Pb ages show that these granitoids were emplaced ~~in~~ two magmatic episodes at ca. 3.47-3.44 Ga and 3.37-3.26 Ga. The volcanic rocks in the greenstone belts of the eastern Singhbhum craton are basalt to basaltic andesite with rare komatiite, whereas in the western Singhbhum craton they are basaltic-andesite to andesite. The whole rock Sm-Nd regression lines for ~~the~~ samples ~~of volcanic rocks~~ from east (including komatiite) and west yield ages of 3746±340 Ma (MSWD = 169) and 2961±420 Ma (MSWD = 3.3), respectively. The major-trace element data show that the volcanic rocks of the eastern and western Singhbhum were derived from two distinct sources. The Paleoarchean granitoids are highly evolved with SiO_2 contents upto 75.86 wt.%. The major and trace element data indicate that the granitoids of the Singhbhum craton were derived by partial melting of a basaltic-andesitic crust at variable depths ~~corresponding to the pressures of~~ ca. 10-15 kbar. ~~Compositions of common Pb measured on~~ leached K-feldspars from the Paleoarchean granitoids show mantle-like characteristics and negate the possible recycling of much older crust into the mantle before formation of these rocks. The whole rock initial Nd isotopic compositions (εNd_i = -0.2 to +2.2) and zircon in-situ initial Hf isotopic compositions (εHf_i = -0.5 to +2.1) of the granitoids calculated using ~~U-Pb zircon~~ ages indicate that they were derived from a near-chondritic reservoir. These data suggest that only a limited volume of felsic crust formed prior to ca. 3.5 Ga, and major crust extraction from the mantle happened at ca. 3.5 Ga. Using this time as the start or major crustal growth and concomitant mantle depletion, Nd and Hf mantle depletion histories are proposed that can be described by the equations εNd_T = -2.78 x (T_{Ga}) + 10, and εHf_T = -4.56 x (T_{Ga}) + 16.4. These curves will not change the model ages for the young rocks, but, they will make a significant difference for the old samples.

Keywords

1. Introduction

The continental crust is the "end product" of the differentiation of the Earth's mantle. The oldest known continental crust formed more than 4 Gyr ago (e.g. Bowring and Housh, 1995) and crustal growth models suggest that at least 60% volume of the continental crust had formed by the end of the Archean (e.g., Taylor and McLennan, 1995). The oldest crustal rocks record ~~history of the~~ chemical differentiation of the early Earth's mantle and therefore can be used to track the crust extraction and mantle depletion during the Hadean and Archean. Whether formation and recycling of the crust happened on early Earth, as it does today, remains unanswered, thus the amount and extent of early formed crust remains obscure. Key questions relate to the timing for the onset of formation of the continental crust and its growth through time (e.g. Hurley and Rand, 1969; Armstrong, 1991; Bennett et al., 1993; Moorbath et al., 1997; Condie, 2000; Harrison et al. 2005; Kemp et al., 2006; Rollinson, 2008; Belousova et al., 2010; Korenaga, 2013; O'Neil et al., 2016; Rosas and Korenaga, 2018). Armstrong (1991) suggested that most, or all, of the continental crust was formed soon after formation of the Earth and underwent multiple recycling events ever since. However, others have argued for episodic growth of the continental crust (e.g. McCulloch and Bennet, 1994; Condie, 1998; Rino et al., 2004).

Many studies have highlighted the strength of the application of multiple isotopic proxies in extracting information about the evolutionary history of the crust-mantle interaction during the Hadean and Archean eons (e.g. DePaolo and Wasserburg, 1976a, b; Jacobsen and Wasserburg, 1980; Patchett et al., 1981; Vervoort et al., 1996; Blichert-Toft and Albarède, 1997, 2008; Nägler and Kramers, 1998; Rino et al., 2004; Tolstikhin et al., 2006; Scherer et al., 2007; Zeh et al., 2007, 2008; Dey, 2013, 2017; Bauer et al., 2017). One of the principal problems in understanding Precambrian geological processes is that only a tiny amount of old (> 3.6 Ga) continental crust is preserved today. Later tectonometamorphic overprinting of the Archean rocks makes it even more challenging to study their genesis. Present day exposed "Hadean" to Paleoarchean crustal masses include the ~~purported~~ ca. 4.3 Ga Nuvvuagittuq greenstone belt (O'Neil et al., 2008), the ~~supposedly~~ 4.03 Ga Acasta gneisses in the Canadian Shield (Stern and Bleeker, 1998), Archean terranes (3.8-3.6 Ga) in Greenland (e.g. Black et al., 1971; Moorbath et al., 1972; Baadsgaard, 1976; Compston et al., 1986; Bennett et al., 1993; Nutman et al.,

95   1999), ca. 3.7 Ga components in the Yilgarn craton (e.g. Myers, 1988; Pidgeon and

96   Wilde, 1990), isolated Hadean (4.4 Ga) zircon grains from the Jack Hills in the

97   Australian Shield (Wilde et al., 2001), ca. 3.5 Ga Barberton greenstone belt (e.g. de

98   Wit et al., 1987; Kröner and Todt, 1988; Armstrong et al., 1990; Kamo and Davis,

99   1994; Kröner et al., 1996; Kröner et al., 2016), ca. 3 Ga components in the

100 Brazilian Shields (e.g. Pidgeon et al., 2000; Santos et al., 2000), North China

101 craton (e.g. Liu et al., 1992, 2008), and Archean (3.6-3.3 Ga) Indian cratons (e.g.

102 Mishra et al., 1999; Ghosh, 2004; Devaraju et al., 2007; Acharyya et al., 2010; Tait

103 et al., 2011; Kaur et al., 2014; Nelson et al., 2014; Upadhyay et al., 2014; Dey et

104 al., 2017). To understand the evolution of the crust on the early Earth, numerous

105 isotopic (e.g. Pb-Pb, Sm-Nd, Lu-Hf) studies have been conducted on the Archean

106 terranes such as SW Greenland which have undergone multiple phases of post-

107 emplacement metamorphism (e.g. Bennett et al., 1993; Vervoort et al., 1996;

108 Moorbath et al., 1997; Nutman et al., 1999; Fisher and Vervoort, 2018), Kaapvaal

109 craton (e.g. Wilson and Carlson, 1989; Kröner et al., 1996; Schoene et al., 2009,

110 Zeh et al., 2013), and Acasta gneisses (e.g. Bowring and Housh, 1995; Iizuka et

111 al., 2009; Bauer et al., 2017). It has been demonstrated in many studies that

112 metamorphic overprinting of Archean rocks can disturb their pristine isotopic (e.g.

113 Sm-Nd) signatures (e.g. McCulloch and Black, 1984; Windrim et al., 1984; Black

114 and McCulloch, 1987; Whitehouse, 1988; Bridgwater et al., 1989; Li et al., 1990;

115 Tourpin et al., 1991; Gruau et al., 1992; Frost and Frost, 1995; Lahaye et al., 1995;

116 Poitrasson et al., 1995; Gruau et al., 1996; Moorbath et al., 1997). Therefore,

117 Archean rocks that are unaffected by any late, post-emplacement, major

118 metamorphic events, are very important for early crustal evolution studies.

119 The Singhbhum craton in eastern India assumes significance as it is one of the

120 oldest cratonic nuclei which exposes a diverse geological association of

121 Paleoarchean to Neoarchean, well preserved and pristine rocks, thus ideally suited

122 for understanding Archean crustal evolution. The craton contains large regions of a

123 Paleoarchean (ca. 3.6-3.3 Ga) sialic crust that was cratonized at around 3.1 Ga

124 (e.g. Mishra et al., 1999; Acharyya et al., 2010; Tait et al., 2011; Nelson et al.,

125 2014; Upadhyay et al., 2014; Dey et al., 2017).

126 This study combines whole rock major-trace element, and Sr-Nd isotope data;

127 leached K-feldspar common Pb isotope data; and in-situ zircon Hf isotope and U-

128   Pb age data from the Paleoarchean granitoids and volcanic rocks of the
129   Singhbhum craton to characterize their source and evolution.

130   **2. Geological setting**

131   The Indian landmass houses four major Archean cratons, including the Dharwar,
132   Aravali-Bundelkhand, Bastar, and Singhbhum craton. The Singhbhum craton in
133   eastern India (Fig. 1) comprises some of the oldest, well preserved and easily
134   accessible Archean lithological units of India. The craton covers an area of ca.
135   40,000 km^2 and is bordered by the Eastern Ghats Belt to the southeast, the Bastar
136   craton to the southwest, and the North Singhbhum Mobile Belt to the north. Three
137   major components that make up the craton are up to amphibolite facies, meta-
138   sedimentary and meta-igneous rocks of the Older Metamorphic Group (OMG),
139   trondhjemite-tonalite-granodiorites (TTGs) of the Older Metamorphic Tonalite
140   Gneisses (OMTG), and granitoids of the Singhbhum Granite (SG) batholith (Saha,
141   1994; Mukhopadhyay, 2001; Upadhyay et al., 2014; Dey et al., 2017). The granitoid
142   nucleus of the Singhbhum craton is enveloped by various supracrustal
143   assemblages with poorly constrained ages.

144   2.1.   Components of the Singhbhum craton
145   2.1.1. Older Metamorphic Group (OMG)

146   The OMG has been considered the oldest component of the craton and has been
147   intruded synkinematically by the OMTG (Saha, 1994; Mukhopadhyay, 2001). The
148   OMG comprises para- and ortho-amphibolites, quartz-sillimanite to quartz-
149   muscovite schists, biotite-muscovite schists, quartz-magnetite-cummingtonite
150   schists, metapelites, quartzites, and banded calc-gneisses (Ray et al., 1987; Saha,
151   1994; Mukhopadhyay, 2001; Hofmann and Mazumder, 2015). The ^{207}Pb-^{206}Pb ion
152   microprobe zircon ages from the OMG metasediments scatter between 3.63 and
153   3.20 Ga but cluster around 3.55, 3.40, 3.35, and 3.20 Ga (Basu at al., 1993;
154   Goswami et al., 1995; Mishra et al., 1999). Based on zircon single grain Pb-Pb
155   ages, Goswami et al. (1995) and Mishra et al. (1999) suggested ~3.5 Ga to be the
156   older limit for the ages of the OMG sediment deposition. The younger 3.40, 3.35
157   and 3.20 Ga ages have been interpreted as metamorphic events (Basu at al., 1993;
158   Mishra et al., 1999; Upadhyay et al., 2014).

159   2.1.2. Older Metamorphic Tonalite Gneisses (OMTG)

160   The OMTG ~~contains~~ greenschist to amphibolite facies tonalite, trondhjemite, granodiorite, and granite (Saha, 1994; Mukhopadhyay, 2001; Misra, 2006).

162   Acharyya et al. (2010) reported two U-Pb zircon ages of 3448±19 Ma (2σ) and 3527±17 Ma (2σ) from the least studied OMTG enclave in the northern area of the Singhbhum craton (Fig. 1). In more recent studies, U-Pb zircon ages ranging from 3.47 Ga to 3.28 Ga have been reported (Nelson et al., 2014; Upadhyay et al., 2014). Upadhyay et al. (2014) demonstrated that tonalites and trondhjemites of the OMTG were emplaced at ca. 3.45-3.44 Ga, whereas granites belonging to the OMTG were emplaced later at ca. 3.35-3.32 Ga.

169   2.1.3. Singhbhum Granite (SG) batholith

170   The SG batholith is the most widespread unit of the Singhbhum craton and occupies an area of about ~8000 km^2 (Saha, 1994). The batholith hosts a suite of biotite-granodiorite/granite, adamellitic granite, trondhjemite and tonalite (Saha, 1984; Mukhopadhyay, 2001; Misra, 2006). Based on field studies, color index and modal mineralogy, Saha (1994) proposed that the SG batholith was emplaced in three phases viz. Phase I, II, III (henceforth SG-I, SG-II, SG-III), SG-I and SG-III being oldest and youngest, respectively. Saha (1994) described SG-I rocks as K-poor granodiorites-trondhjemites (mean modal composition in volume percent; Pl: 55.2%, Kfs: 6.7%, Qz: 30.1%, Bt: 2.8%, Ep-Zo+Chl: 4.9%, Ms: 0.1%, An content of Pl: 15.28), whereas SG-II rocks (Pl: 49.2%, Kfs: 15.6%, Qz: 28.2%, Bt: 1.5%, Ep-Zo+Chl: 4.6%, Ms: 0.15%, An content of Pl: 13.32) and SG-III rocks (Pl: 44.5%, Kfs: 18.3%, Qz: 30.2%, Bt: 1.9%, Ep-Zo+Chl: 3.8%, Ms: 0.7%, An content of Pl: 8.22) as granodiorites to adamellitic granites (mineral abbreviations after: Whitney and Evans (2010)). Recent U-Pb zircon studies have revealed that rocks of the SG batholith were emplaced between ~3.45 Ga and ~3.32 Ga (Tait et al., 2011; Nelson et al., 2014; Upadhyay et al., 2014; Dey et al., 2017). Based on texturally controlled Laser Ablation Inductively Coupled Plasma Mass Spectrometer (LA-ICP-MS) U-Pb dating of the zircon grains, Upadhyay et al. (2014) suggested that SG-III rocks along with tonalities and trondhjemites of the OMTG were emplaced at ca. 3.45-3.44 Ga, whereas, SG-I and SG-II together with granites of the OMTG were emplaced at ca. 3.35-3.32 Ga.

191   2.1.4. Volcano-sedimentary successions

The Archean Singhbhum granitoid nucleus is surrounded by various volcano-sedimentary assemblages of poorly constrained age such as the Iron Ore Group (IOG) and the Dhanjori-Jagannathpur-Malangtoli lavas (Fig. 1). The IOG is a low-grade greenstone succession comprising banded iron formation, ferruginous quartzite, shale, phyllite, chert, minor carbonates, mafic-felsic volcanic rocks and ultramafic rocks (Saha, 1994; Mukhopadhyay, 2001). These volcano-sedimentary rocks (IOG) occur in three major basins Gorumahisani-Badampahar, Noamundi-Jamda-Koira, and Tomka-Daitari on the eastern, western, and southern margin of the granitoid nucleus, respectively (Fig. 1). Due to paucity of geochronological data from the IOG greenstone successions, the time of their deposition is unclear. However, based on field relationships a minimum age of 3.2-3.1 Ga has been assigned for their deposition (Paul et al., 1991; Mishra et al., 1999). Mukhopadhyay et al. (2008) reported a U-Pb SHRIMP zircon age of 3506.8±2.3 Ma (1σ) for the dacitic lava of the Southern IOG (SIOG; Tomka-Daitari basin). Enclaves of banded iron formation and calc-silicate rocks, presumably derived from the eastern IOG (EIOG; Garumahisani-Badampahar basin) hosted within 3326±5 Ma (1σ) biotite-muscovite monzogranite of the SG batholith near Rairangpur provide a minimum age for the EIOG succession (Nelson et al., 2014). Komatiites from the EIOG have been reported from Patharkata (Sahu and Mukherjee, 2001), Dhipasai (Tua Dungri hillock; Chaudhuri et al., 2015), and Kapili (e.g. Yadav et al., 2015; Chaudhuri et al., 2017) villages. Although no direct geochronological data are available for these komatiites, based on their field relationship with other lithologies an age of ~3.34 Ga has been assigned to the Kapili komatiites by Chaudhuri et al. (2017). The Singhbhum craton hosts some shallow volcano-sedimentary basins viz. Dalma-Dhanjori-Simlipal-Malangtoli and Jagannathpur (Fig. 1). Geochronological and isotopic data from these volcanic rocks present in different basins are scanty, hence the time of their emplacement and their petrogenesis remain unclear.

3. Samples and analytical methods

Representative and best-preserved samples were collected from the OMTG, SG-I, SG-II, SG-III, IOG, Jagannathpur Lava (JL), and Malangtoli Lava (ML). Sample details are given in Table 1.

Samples were crushed in a steel jaw crusher and powdered to ca. 70 µm particle size using agate mortar. Aliquots of 5 mg were taken from all the samples and analyzed by Actlabs Canada for major and trace elements analyses (package

226   code: 4 Lithoresearch). Samples were fused with lithium metaborate/tetraborate

227   and dissolved in 5% HNO_3. All major elements (as oxides) and some trace

228   elements (Sc, V, Sr, Zr, and Ba) were analyzed with an Inductively Coupled Plasma

229   Optical Emission Spectrometer (ICP-OES); whereas, all other trace elements were

230   analyzed with an Inductively Coupled Plasma Mass Spectrometer (ICP-MS).

231   Further analytical details can be found in http://www.actlabs.com. Common Pb,

232   Sm-Nd, and Rb-Sr isotopic measurements were done at the Institute of Geological

233   Sciences, University of Bern, Switzerland.

234   3.1.   Sample preparation for common Pb analysis

235   For common Pb isotopic measurements samples were crushed in a steel jaw

236   crusher and washed with water. The K-feldspars were separated using heavy liquid

237   (mixture of methyl iodide and acetone) and handpicked under the microscope.

238   Handpicked K-feldspar grains were leached in three steps, using an extension of

239   the protocol of Villa et al. (2006) and Villa & Hanchar (2013). This had the purpose

240   of removing all the secondary clays and sericite, as well as external Pb adsorbed

241   on the surface of the grains. In the first step the grains were leached in ~1 ml of

242   aqua regia (mixture of 6.4 M HCl and 7 M HNO_3) on a hotplate in 7ml screw-top

243   PTFE (polytetrafluoroethylene) beakers at 100°C for ca. 15 hours. In the second

244   step the K-feldspars were leached in a mixture of 6.4 M HCl + 7 M HNO_3 (~0.5 ml)

245   and a few drops of weak HF on a hotplate for ca. 3 minutes. In the third step, the

246   grains were leached in a mixture of 6.4 M HCl + 7 M HNO_3 (same amount as in the

247   previous step) and weak HF by putting the vials on the hotplate for ca. 2-3 minutes

248   until ca. 50% of the sample had dissolved. Grains were washed four times with

249   deionized water between each leaching step. Finally, the grains were completely

250   dissolved in few drops of concentrated HF on a hotplate at 100°C for ca. 12-24

251   hours (depending on the rate of dissolution) and then dried. Lead was isolated by

252   using DOWEX® 1-X8 anion resin. Lead isotopes were measured on the Nu

253   Plasma® Multicollector ICP-MS (MC-ICP-MS). For mass bias correction samples

254   were doped with Tl, and [203]Tl, [205]Tl were measured simultaneously with the

255   isotopes of Pb. Interference of [204]Hg on [204]Pb was corrected by monitoring the

256   signal for [202]Hg. Lead isotope ratios were corrected for mass bias using exponential

257   law. Measurements of the common Pb isotopic standard (NIST SRM® 981) yielded

258   [207]Pb/[206]Pb = 0.91470±0.00011 (2σ; n = 6).

259   3.2.   Sample preparation for Sm-Nd and Rb-Sr analyses

260   For Sm-Nd and Rb-Sr isotopic analyses, ca. 100 mg of whole rock powder of each

261   sample were digested in Parr® bombs after adding ^{87}Rb-^{84}Sr and ^{149}Sm-^{150}Nd mixed

262   whole rock spikes. For the complete dissolution of the samples they were

263   processed in several steps. At first, samples were treated with 1.5 ml concentrated

264   (48%) HF and a few drops of 14 M HNO_3 in 3 ml PTFE vials. These vials were then

265   put inside PTFE liners and then into Parr® bombs. Parr® bombs were kept in an

266   oven at 180°C temperature for 48 hours. After the bombs had cooled, the beakers

267   were removed and kept on a hotplate with open lids at 100°C to dry. In the second

268   step, 1.5 ml 2 M HNO_3 was added and beakers were placed on the hotplate with

269   closed lids at 100°C (near boiling) for 6 hours. Then, samples were dried on a

270   hotplate at 100°C. In the third step, 2 ml 2.5 M HCl was added to the samples and

271   they were boiled on the hotplate at 100°C for 1 hour with closed lids. Afterwards,

272   the vials were placed on hotplate with open lids at 100°C until almost dry. Samples

273   with undigested residue were processed again through steps 2 and 3. After this, the

274   samples were completely digested and dissolved in 2 ml 2.5 M HCl by keeping the

275   beakers with closed lids on hotplate at 100°C for 30 minutes. After cooling the

276   samples were loaded on 6 ml DOWEX® AG 50W-X8 (200-400 mesh) cation

277   exchange columns to separate Rb, Sr and Rare Earth Elements (REE). To isolate

278   Sm and Nd, REE fractions were passed through 5 ml HDEHP (di-(2-ethylhexyl)

279   phosphoric acid) columns.

280   Rubidium and Sm concentrations in the spiked samples were measured on Thermo

281   Scientific™ Neptune Plus™ MC-ICP-MS. Neodymium and Sr isotopes were

282   measured on a Thermo Scientific™ Triton Plus™ Thermal Ionization Mass

283   Spectrometer (TIMS) in static mode. Total procedural blanks for all the elements

284   (i.e. Rb, Sr, Sm, and Nd) were <700 pg (i.e. <0.15% of the sample amount) and are

285   thus negligible. Rubidium and Sm isotope ratios were corrected for mass bias

286   (using the exponential law) by the standard-sample-standard bracketing method by

287   measuring JMC Rb and Sm standards. Strontium cuts were loaded in 6.4 M HCl

288   with Ta-fluoride as an activator on zone-refined Re single filaments, whereas Nd

289   fractions were loaded with 6.4 M HCl on zone-refined Re double filaments without

290   any activator. Neodymium and Sr isotope ratios were corrected for mass bias using

291   exponential law and iteration method (Stracke et al. 2014), as samples were

292   spiked. For quality control, isotope ratios of Nd and Sr isotopic standards JNdi-1

293   and NIST SRM® 987 respectively, were measured. The isotopic ratios of Nd and Sr

294   standards were corrected for mass fractionation using exponential law with

295 normalization ratios of $^{146}Nd/^{144}Nd$ = 0.7219 and $^{86}Sr/^{88}Sr$ = 0.1194, respectively.

296 Standards JNdi-1 and NIST SRM® 987 yielded $^{143}Nd/^{144}Nd$ = 0.512067±0.000009

297 (2σ; n = 26) and $^{87}Sr/^{86}Sr$ = 0.710329±0.000011 (2σ; n = 14), respectively.

298 Neodymium and Sr isotope ratios of the samples were corrected for the offset with

299 respect to recommended values for JNdi-1 ($^{143}Nd/^{144}Nd$ = 0.512115; Tanaka et al.,

300 2000) and NIST SRM® 987 ($^{87}Sr/^{86}Sr$ = 0.710245).

301 3.3.   U-Pb zircon dating with LA-ICP-MS

302 Uranium-Pb dating was performed on a Thermo Scientific™ iCAP-Q™ quadrupole

303 ICP-MS coupled with a 193nm ArF excimer laser ablation system, at the

304 Department of Geology and Geophysics, Indian Institute of Technology (IIT),

305 Kharagpur. The ICP-MS was optimized for maximum sensitivity on ^{208}Pb, ^{232}Th and

306 ^{238}U using the NIST SRM® 612 reference glass. The oxide production was

307 monitored on mass 248 ($^{232}Th^{16}O$) and found to be <0.9% during all analytical

308 sessions. The laser was operated at 5 Hz repetition rate, and ca. 5 J/cm^2 beam

309 energy density. The spot size was 35 μm for the GJ-1 and 91500 reference zircons

310 (Jackson et al., 2004; Wiedenbeck et al., 1995) and 30-5 μm for samples. The

311 spots were pre-ablated with five laser pulses prior to analysis to remove any

312 surface contamination. The data were acquired in a time-resolved mode with each

313 analysis consisting of 30 s measurement of instrument background/gas blank with

314 the laser off and 50 s measurement of peak signals with the laser ablating on the

315 sample. Helium was used as a carrier gas (0.55 L/min) to transport the ablated

316 aerosol. The data were reduced offline using an in-house Excel© spreadsheet,

317 which corrects for instrument/gas background, laser-induced elemental

318 fractionation, instrumental mass-bias and drift. The signal for ^{204}Pb was very low

319 (for the analyses used for age calculations), hence no common Pb correction was

320 applied. The ^{235}U was estimated using $^{238}U/^{235}U$ ratio of 137.88. External

321 standardization was done by bracketing ten measurements of the sample with

322 three measurement of GJ-1 reference zircon. The 91500-reference zircon was

323 analyzed as unknown for monitoring data quality. The uncertainty on each spot

324 analysis was estimated by quadratic addition of the $2σ_m$ (standard error on the

325 mean) internal run statistics of each analysis, and the 2σ (standard deviation) of the

326 ratios measured in the bracketing standard (GJ-1). The measured $^{206}Pb/^{238}U$

327 (0.179±0.004, 2σ) and $^{207}Pb/^{206}Pb$ (0.0748±0.0007, 2σ, n=18) match recommended

328 values (Wiedenbeck et al., 1995). The U content of the zircons were estimated

329 relative to the GJ-1 reference zircon. Concordia diagrams were constructed using

330 Isoplot 4.15 (Ludwig, 2003).

331 ### 3.4. Zircon in-situ Hf isotope analysis

332 Hafnium isotopes were measured on a Thermo Scientific™ Neptune Plus™ MC-

333 ICP-MS coupled with same laser ablation system used for the U-Pb dating. All

334 analyses were done at a laser spot size of 50 μm. The 91500 reference zircon was

335 used as an external bracketing standard with ten measurements of the samples

336 bracketed with three measurements of the 91500 zircon. The laser was operated at

337 10 Hz repetition rate, and 4.5-5 J/cm^2 beam energy density. The data were

338 acquired in time-resolved mode with 30 s of background measurement without the

339 laser firing and 55 s of peak signal measurement with the laser on using an

340 integration time of 0.524 s per cycle. The isobaric interference of ^{176}Yb and ^{176}Lu on

341 ^{176}Hf were corrected using the peak stripping method. For Yb, the isobaric

342 interference correction was done using the values reported by Thirlwall and

343 Anczkiewicz (2004). The mass-bias factor for Yb isotopes (β_{Yb}) was calculated

344 using the exponential law from the measured ^{173}Yb/^{171}Yb. The mass-bias factor for

345 Hf (β_{Hf}) was calculated using exponential law from the measured ^{179}Hf/^{177}Hf ratio

346 (recommended value of 0.7325; Patchett et al., 1981). The isobaric interference of

347 ^{176}Lu on ^{176}Hf was corrected using the interference free ^{175}Lu isotope and the

348 natural ^{176}Lu/^{175}Lu value of 0.02656 (Chu et al., 2002). The mass-bias factor for Lu

349 is assumed to be identical to that of Hf (i.e., $\beta_{Lu} = \beta_{Hf}$). The uncertainties on each

350 spot were estimated by quadratic addition of the within run precision (2SE) of each

351 analysis and the reproducibility (2SD) of the bracketing standard 91500. The

352 accuracy and external reproducibility of the method was tested by measuring the

353 Temora-2 (Black et al., 2004) and Plešovice (Sláma et al., 2008) reference zircons

354 as unknown. The measured ^{176}Hf/^{177}Hf values of Temora-2 and Plešovice zircon

355 reference zircons range from 0.282641 to 0.282688 (mean = 0.282669±37 (2σ

356 (1.3ε), n = 5)) and 0.282460 to 0.282486 (mean= 0.282479±26 (2σ (0.9ε), n = 4)),

357 respectively. Despite spread, the mean ^{176}Hf/^{177}Hf values of Temora-2 and

358 Plešovice zircon agree (within uncertainty) with the accepted values

359 (^{176}Hf/^{177}Hf$_{Temora-2}$ = 0.282686±8 (2σ), and ^{176}Hf/^{177}Hf $_{Plešovice}$ = 0.282482±12 (2σ);

360 Fisher et al., 2014).

361 For the calculation of the εHf_i, the chondritic uniform reservoir (CHUR) value of

362 Bouvier et al. (2008) ($^{176}Lu/^{177}Hf$ = 0.0336 and $^{176}Hf/^{177}Hf$ = 0.282785), and ^{176}Lu

363 decay constant of 1.867×10^{-11} a^{-1} (Scherer et al., 2001; Söderlund et al., 2004)

364 were used. Initial $^{176}Hf/^{177}Hf_i$ and εHf_i for all the analysed grains were calculated

365 using either concordia ages or the $^{207}Pb/^{206}Pb$ ages of the respective samples. The

366 error propagation and the uncertainties on the initial $^{176}Hf/^{177}Hf_i$ ratios and εHf_i are

367 after Ickert (2013). Further instrumental details are presented in Appendix A1.

4. Results

369 The whole rock major-trace element, Sm-Nd isotope, and Rb-Sr isotope data are

370 listed in Table 2, Table 4, and Appendix A3, respectively. Common Pb isotope data

371 for leached K-feldspars, single zircon U-Pb dating, and zircon in-situ Hf isotope

372 data are given in Table 3, Appendix A2, and Appendix A4 (mean of εHf_i for each

373 sample in Table 5), respectively.

4.1. Whole rock major-trace elements

4.1.1. Granitoids

376 Most of the granitoids of the Singhbhum craton fall in the trondhjemite and granite

377 field in the albite-orthoclase-anorthite ternary plot of Barker (1979), except sample

378 Om 23 (SG-I) which is a tonalite (Fig. 2a). Whole rock major-trace elements data

379 are given in Table 2. The SiO_2 content of trondhjemites and granites range from

380 67.76 to 74.73 wt.% and 72.07 to 75.86 wt.% respectively; whereas tonalite (Om

381 32) has 65.84 wt.% SiO_2 (concentrations normalized to 100% after correcting for

382 loss on ignition). Trondhjemite and tonalite have higher Na_2O, Al_2O_3, CaO, MgO,

383 MnO, TiO_2, $Fe_2O_3(T)$, and Sr; and lower K_2O contents compared to granites (Fig.

384 3). Most granitoid samples show a trend of decreasing Na_2O, Al_2O_3, CaO, MgO,

385 MnO, TiO_2, $Fe_2O_3(T)$, and Sr with increasing SiO_2 in Harker diagrams (Fig. 3);

386 whereas K_2O displays a positive trend against SiO_2 (Fig. 3). The granitoids show

387 the REE composition ranging from high HREE content (La/Yb = 10.94) to low

388 HREE content (La/Yb = 147.39; Fig. 3, Table 2).

389 In the chondrite normalized REE diagrams (Sun and McDonough, 1989),

390 trondhjemite, granite, and tonalite show enriched light-REE (LREE) and depleted

391 heavy-REE (HREE) patterns with a steep slope for LREE and gentler for the HREE

392 (Fig. 4). Trondhjemite of OMTG do not show any significant Eu anomaly (Eu/Eu* =

393   0.83–1.16); whereas, trondhjemite of SG batholith display both positive and

394   negative Eu anomaly (Eu/Eu^*_{SG-II} = 0.65–0.94; and Eu/Eu^*_{SG-III} = 0.51–1.27; Figs.

395   4a, c, d). One of granite samples from OMTG (Om 30a) shows a smooth REE

396   pattern without any Eu anomaly (Eu/Eu^* = 1.01), whereas the other (Om 11b) has a

397   pronounced negative Eu anomaly (Eu/Eu^* = 0.45; Fig. 4a). The granites of SG-II

398   have a slightly negative to a slightly positive Eu anomaly (Eu/Eu^* = 0.77–1.22; Fig.

399   4c), whereas granites belonging to SG-III show both negative and positive Eu

400   anomalies (Eu/Eu^* = 0.27–1.91) and have large spread in HREE concentrations

401   (Fig. 4d). Trondhjemite and granite with negative Eu anomaly are less depleted in

402   HREE compared to those with a positive or no Eu anomaly (Figs. 4a, c, d). Tonalite

403   (Om 32; SG-I) shows smooth LREE enriched-HREE depleted pattern with no Eu

404   anomaly (Eu/Eu^* = 0.99; Fig. 4b). Sample (Om 2a) from a gabbroic-diorite xenolith

405   in SG-II has a gentle REE pattern with Eu/Eu^* = 0.99 (Fig. 4c), whereas a diorite

406   (Om 10b) from the SG-III association shows a relatively steeper REE pattern with a

407   slight negative Eu anomaly (Eu/Eu^* = 0.79; Fig. 4d). All rock types display

408   differently pronounced negative Nb, Ta, and Ti; and positive K (except Om 32; SG-

409   I; tonalite; Fig. 4f), and Pb anomalies in primitive mantle (Sun and McDonough,

410   1989) normalized multi-element diagrams (Figs. 4e–h).

411   4.1.2. Volcanic rocks

412   Fourteen volcanic rocks were selected for this study (4 from EIOG, 3 from western

413   IOG (WIOG, Noamundi-Jamda-Koira basin), 1 from JL, and 4 from ML) including 2

414   samples of komatiite (OPP 10a & OPP 10b; from EIOG) from the Singhbhum

415   craton (see Table 1 and Fig. 1). For simplicity of the figures, volcanic rocks from the

416   western part of the craton (i.e. WIOG, JL, and ML) have been grouped as 'West

417   Singhbhum Volcanic Rocks' and volcanic rocks from the eastern part (i.e. EIOG)

418   have been grouped as 'East Singhbhum Volcanic Rocks'. Komatiites from the

419   EIOG are grouped as 'East Singhbhum Komatiite'.

420   In the total-alkali-silica (TAS) diagram after Le Maitre et al. (1989), samples

421   belonging to the West Singhbhum Volcanic Rocks fall in the basaltic-andesite to

422   andesite field; whereas samples belonging to East Singhbhum Volcanic Rocks and

423   East Singhbhum Komatiite fall within the basalt to basaltic-andesite field (Fig. 2b).

424   Whole rock major-trace element data is presented in Table 2. West Singhbhum

425   Volcanic Rocks have Al_2O_3 and $Fe_2O_3(T)$ contents (after correcting for loss on

426   ignition) between 10.53–13.41 wt.%, and 8.78–11.28 wt.%, respectively. East

Singhbhum Volcanic Rocks have lower Al_2O_3 (6.25–8.35 wt.%) and higher $Fe_2O_3(T)$ (12.69–13.63 wt.%). The K_2O, Na_2O, Al_2O_3, Sr, and Zr of the volcanic rocks show a positive correlation with SiO_2 (Fig. 3). For most of the samples the concentration of CaO, MgO, MnO, and $Fe_2O_3(T)$ decreases with increasing SiO_2 content (Fig. 3).

The West Singhbhum Volcanic Rocks show a slightly LREE enriched and HREE depleted pattern with a negative Eu anomaly (Eu/Eu* = 0.52–0.89) in a chondrite normalized REE diagram (Fig. 5a; Table 2). The East Singhbhum Volcanic Rocks display almost flat REE pattern with slightly enriched LREEs and no significant Eu anomaly (Eu/Eu* = 0.89–1.04; Fig. 5a; Table 2). The East Singhbhum Komatiites are least depleted in REE compared to the other volcanic rocks; however, they show slight La and Ce enrichment and HREE depletion with Eu/Eu* = 0.87–1.05 (Fig. 5a; Table 2). In a primitive mantle normalized multi-element plot (Fig. 5b) the West Singhbhum Volcanic Rocks have negative Nb, and Ti anomalies; and most of the rocks have positive K and Pb anomalies. Komatiites and other volcanic rocks from the East Singhbhum Volcanic Rocks display a variable degree of negative Ba, and Nb anomalies (Fig. 5b).

4.2.   Common Pb isotope in leached K-feldspars

Initial Pb isotope compositions of 14 granitoid samples of the Singhbhum craton were determined on leached K-feldspars. Measured Pb isotope data are reported in Table 3 and plotted in Fig. 6. In $^{206}Pb/^{204}Pb$ vs. $^{208}Pb/^{204}Pb$ and $^{206}Pb/^{204}Pb$ vs. $^{207}Pb/^{204}Pb$ diagrams, Pb isotopic composition of the studied samples cluster closely around the model Pb evolution curve of Kramers and Tolstikhin (1997), which, for the Paleoarchean, is almost identical to the simplified precursor model by Stacey and Kramers (1975). The Pb model ages of the leached feldspars are ca. 3.3-3.1 Ga (Fig. 6). For comparison, Pb isotope data for the Archean rocks from West Greenland (Kamber and Moorbath, 1998; Kamber et al., 2003; leached feldspars) and the Barberton greenstone belt (Ulrych et al., 1967; Sinha and Tilton, 1973; galena, jamesonite, and unleached feldspar) are also plotted and show a large scatter compared to the results from the Singhbhum craton (Fig. 6).

4.3.   Single zircon U-Pb LA-ICP-MS dating

Zircon grains separated from eight selected granitoid samples were used for in-situ Hf and U-Pb isotope analyses. Cathodoluminescence (CL) images of some of the analysed zircon grains are presented in Fig. 7. Laser ablation spots for U-Pb and Hf

isotopic analyses are marked with solid and dotted circles, respectively. Data for individual U-Pb analyses are reported in Appendix A2 and are plotted in concordia diagrams in Fig. 8. Uncertainties on all ages presented in this study are 2σ.

The two trondhjemite samples Om 11a and Om 29 from OMTG yielded concordant U-Pb zircon ages of 3274±17 Ma and 3352±13 Ma respectively (Figs. 8a, b). One zircon grain (Om 29_19; Fig. 7) from sample Om 29 has a $^{207}Pb/^{206}Pb$ age of 3440±37 Ma (Fig. 8b) and is interpreted as inherited zircon age. Zircons from granite sample (Om 11b) from OMTG have concordant U-Pb age of 3304±15 Ma; however an inherited zircon grain Om 11b_6 (Fig. 7) yielded a $^{207}Pb/^{206}Pb$ age of 3472±57 Ma (Fig. 8c). Trondhjemite sample (Om 5b) from SG-II yielded concordant U-Pb age of 3335±19 Ma which is similar to the upper intercept age of the discordia line (Fig. 8d). Zircons from granite (Om 22) of SG-II have a concordant U-Pb age of 3327±19 Ma (Fig. 8e). The trondhjemite sample Om 12 from SG-III yielded a concordia age of 3470±19 Ma (Fig. 8f); whereas, zircons from sample Om 18 neither yield a concordia U-Pb date nor define a discordia, hence the oldest and least discordant $^{207}Pb/^{206}Pb$ age of 3263±26 Ma (Fig. 8g; Appendix A2) has been assigned to this sample. Zircon grains from granite (Om 15) of SG-III have a concordia U-Pb age of 3352±10 Ma (Fig. 8h). All these ages (except from inherited zircons grains/cores) are interpreted as emplacement ages for their respective rocks.

4.4. Whole rock Nd and Sr isotopes

4.4.1. Granitoids

Whole rock Sm-Nd isotope composition of the older (except Om 12) and younger (Om 11a) granitoids (OMTG, SG-I, II, III) form alignments with significant scatter ($MSWD_{older}$ = 258; $MSWD_{younger}$ = 1097). The apparent ages of these alignments are 3344±160 Ma and 3142±390 Ma with initial εNd values of -0.2 and -1.4, respectively (Fig. 9a & b). These ages are in broad agreement (within uncertainties) with reported U-Pb zircon ages (e.g. Upadhyay et al., 2014) and those presented in this study (Appendix A2, Fig. 8) for the granitoids of the Singhbhum craton. The initial $^{143}Nd/^{144}Nd$ ratios and εNd for the dated samples have been calculated using their respective U-Pb zircon ages presented in Fig. 8; whereas, those for other granitoid samples are calculated based on U-Pb zircon ages reported in Upadhyay et al. (2014) (Table 4).

493 Most of the samples have near-chondritic initial εNd ~~and/or isotope ratios~~ close to

494 ~~the values~~ corresponding to some of the proposed mantle depletion model curves

495 (e.g. DePaolo, 1981; Nägler and Kramers, 1998). The ~~initial~~ $^{143}Nd/^{144}Nd$ values for

496 the older granitoids (3440 Ma) range from ~~0.508165 (εNd$_i$ = +0.1) and~~ 0.508273

497 (εNd$_i$ = +2.2). The younger granitoids (3263 Ma - 3363 Ma) have initial $^{143}Nd/^{144}Nd$

498 values between 0.508269 (εNd$_i$ = -0.2) and 0.508477 (εNd$_i$ = +1.6). Some samples

499 such as Om 12 (3470 Ma), Om 11a (3374 Ma), Om 5b (3335 Ma), and Om 22

500 (3327 Ma) have higher εNd$_i$ values of +5.2, +4.8, +3.2, and +2.6, respectively

501 (Table 4, Fig. 10a).

502 The calculated initial $^{87}Sr/^{86}Sr$ for the older granitoids range from 0.634132 (Om 17)

503 to 0.717160 (Om 12)$_{\bar{i}}$ whereas$_{\bar{i}}$ the younger intrusive suite has initial $^{87}Sr/^{86}Sr$

504 values between 0.683335 (Om 11b) and 0.711441 (Om 2b) (Appendix A3). The

505 large spread of the initial $^{87}Sr/^{86}Sr$ values and the presence of values lower than the

506 solar system initial (~0.699) indicate post-emplacement disturbance of the Rb-Sr

507 system, which has a large effect on the calculated initial Sr-isotope ratios due to the

508 high Rb/Sr ratios in these rocks (e.g. $^{87}Rb/^{86}Sr$ = 6.164 for Om 17). Just a 1%

509 change in $^{87}Rb/^{86}Sr$ (6.164) changes the initial $^{87}Sr/^{86}Sr$ by 48ε indicating even a

510 slight modification in Rb/Sr ratio leads to the erroneous initial $^{87}Sr/^{86}Sr$ value.

511 Hence, the Sr isotope data does not yield robust initial $^{87}Sr/^{86}Sr$ for these rocks.

512 4.4.2. Volcanic rocks

513 Whole rock Sm-Nd isotope data for the East Singhbhum Volcanic Rocks (including

514 East Singhbhum Komatiite) and the West Singhbhum Volcanic Rocks (except Om

515 37, Om 42, Om 43) define regression lines corresponding to 3746±340 Ma (MSWD

516 = 169) and 2961±420 Ma (MSWD = 3.3), with initial εNd values of +2.7 and +0.2,

517 respectively (Fig. 9c & d). However, in the absence of other direct radio-isotopic

518 ages for these rocks, robust initial εNd values for individual samples cannot be

519 constrained; and initial εNd values obtained from regression lines with high MSWD

520 also cannot be considered robust. West Singhbhum Volcanic Rocks have lower

521 $^{147}Sm/^{144}Nd$ (present day) ratios (0.1275–0.1353), whereas East Singhbhum

522 Volcanic Rocks have significantly higher values (0.1437–0.2053) (Table 4; Fig. 9c

523 & d).

524 The present day $^{87}Rb/^{86}Sr$ and initial $^{87}Sr/^{86}Sr$ ratios (calculated using Sm-Nd

525 regression line ages) for these rocks range from 0.0110 to 1.591 and 0.667480 to

526 0.709015, respectively (Appendix A3). The spread of initial $^{87}Sr/^{86}Sr$ ratios over a
527 large range and most of them being below ca. 0.699 (solar system initial) confirm
528 some post-emplacement modification of the initial Rb/Sr ratios, which led to the
529 erroneous calculated values of initial Sr isotopic composition. Hence, these Sr
530 isotope data have not been used for petrogenetic interpretation.

531 4.5.   Zircon in-situ Hf isotopes

532 Hafnium isotopes in single zircon grains from eight granitoid samples were
533 measured using LA-MC-ICP-MS and data for individual grain analyses are
534 presented in Appendix A4. The samples with high initial εNd values (+5.2 – +1.6;
535 depleted mantle signature) along with two samples, Om 29 ($εNd_i$ = +0.5) and Om
536 15 ($εNd_i$ = +1.1) with near chondritic values, were selected for Hf isotope analysis.

537 Individual zircon grains from the same sample (with the same age) show an intra-
538 sample spread in their initial εHf values of 2 to 6 ε units. Sample Om 5b shows the
539 lowest spread ($εHf_{3335\ Ma}$ = 0 – +2.2), whereas sample Om 12 shows the largest
540 spread ($εHf_{3470\ Ma}$ = -2.5 – +3.8; Appendix A4). Despite this spread in the measured
541 $^{176}Hf/^{177}Hf$ values of the reference zircons Temora-2 and Plešovice, their mean are
542 in the agreement with the accepted values. Therefore, the mean of the initial εHf
543 values of individual zircon grains of the same sample has also been considered to
544 be the representative of the initial εHf of the specific sample. The mean εHf values
545 for all the samples have been reported in Table 5. The errors reported on the mean
546 $εHf_i$ are the 2 x standard error ($2σ_m$) on the mean.

547 The initial εHf values for most of the analyzed samples are near-chondritic ranging
548 from -0.5±0.8 ($2σ_m$, n = 9) to +2.1±0.6 ($2σ_m$, n = 14). The samples with high initial
549 εNd values, such as Om 12 ($εNd_{3470\ Ma}$ = +5.2), Om 11a ($εNd_{3374\ Ma}$ = +4.8), Om 5b
550 ($εNd_{3335\ Ma}$ = +3.2), and Om 22 ($εNd_{3327\ Ma}$ = +2.6), yielded initial εHf values of
551 +0.1±1.1 ($2σ_m$, n = 11), +1.5±1.0 ($2σ_m$, n = 6), +1.4±0.4 ($2σ_m$, n = 10), and +0.7±0.9
552 ($2σ_m$, n = 11) respectively (Table 5, Fig. 10b). In an $εHf_i$ vs. age (Hf mantle
553 depletion) diagram, the scatter of the data from the individual analyses have been
554 marked with the yellow shaded region, which spreads from the sub-chondritic to the
555 conventional mantle depletion line. However, the mean $εHf_i$ of each sample clusters
556 well below the mantle depletion line (Fig. 10b).

557 **5. Discussion**

5.1. Major-trace element constraints on the petrogenesis

The high SiO_2 content (as high as 75.86 wt.%) of the granitoids from the Singhbhum craton shows that they are highly evolved. The correlation of decreasing Na_2O, Al_2O_3, CaO, MgO, MnO, and $Fe_2O_3(T)$, TiO_2, Sr, and increasing K_2O with increasing SiO_2 content (Fig. 3), hint towards the derivation of these granitoids by differentiation of chemically and mineralogically similar source(s) followed by similar differentiation processes (i.e. partial melting and/or fractional crystallization). The chondrite, and primitive mantle (Sun and McDounough, 1989) normalized REE, and multi-element patterns (Fig. 5) of the West Singhbhum Volcanic Rocks (basaltic-andesite to andesite) differ from the East Singhbhum Volcanic Rocks (basalt to basaltic-andesite) and East Singhbhum Komatiite. The East Singhbhum Volcanic Rocks along with the East Singhbhum Komatiite have almost flat REE patterns without any significant Eu anomaly, a negative K anomaly and Pb below detection limit (<5 ppm); whereas, the West Singhbhum Volcanic Rocks have slightly fractionated REE patterns with negative Eu anomalies, and positive K and Pb anomalies (Fig. 5). The difference indicates that the West Singhbhum Volcanic Rocks, and the East Singhbhum Volcanic Rocks (including East Singhbhum Komatiite) are derived from two different sources. The granitoids have multi-element patterns similar to the West Singhbhum Volcanic Rocks (Figs. 4e-h, 5b). This is consistent with the granitoids being derived by partial melting of lower crust with a composition similar to the West Singhbhum Volcanic Rocks (i.e. basaltic-andesite to andesite), but the ultimate source (i.e. upper mantle) itself was enriched in K and Pb. The compositional gap between the West Singhbhum Volcanic Rocks and the granitoids in bivariate plots (Fig. 3) also indicates that the granitoids are the product of partial melting rather than fractional crystallization of mafic melt. In the Sr vs. SiO_2, Nb vs. Ta, La/Yb vs. Yb, and Sr/Y vs. Y diagrams (Fig. 3), the Singhbhum granitoids range from 'high pressure' (at least 15 kbar; low-HREE, i.e. high La/Yb) to the low pressure (ca. 10-12 kbar; high-HREE, i.e. low La/Yb) field; however most of them fall in medium to low pressure category (see Hoffmann et al., 2011; Moyen, 2011; Moyen and Martin, 2012). Hence, it is interpreted that the Singhbhum granitoids are derived by the melting of a mafic crust at variable depths corresponding to the pressure range of ca. 10-15 kbar. The variable degree of negative to positive Eu anomalies observed in these granitoids can be the result of plagioclase fractionation or accumulation during fractional crystallization of the melt.

593 The similar element patterns observed in the granitoids and the West Singhbhum
594 Volcanic Rocks indicates that they may be derived ultimate from the same source,
595 but at different times. The two rock suites were not produced by the same melting
596 event, because the granitoids (ca. 3.5-3.2 Ga) are older than the West Singhbhum
597 Volcanic Rocks (ca. 2.96 Ga, Fig. 9d) and are derived by partial melting of lower
598 crust. The high Cr (330-1380 ppm) and Ni (130-460 ppm) contents of the West
599 Singhbhum Volcanic Rocks attest to their derivation from primitive mantle derived
600 melts. Therefore, their positive K and Pb anomalies, which are also observed in the
601 granitoids, are a mantle signature. Thus, it is possible that the source rocks of the
602 older granitoids originate from a mantle reservoir that is chemically similar to the
603 source of the younger volcanic rocks in this region.

604 The similarity of the high Ni and Cr contents of the East Singhbhum Volcanic Rocks
605 (Ni = 240-800 ppm, Cr = 760-2520 ppm) and East Singhbhum Komatiite (Ni =
606 1680-2070 ppm, Cr = 1240-1680 ppm) and almost flat REE patterns (Fig. 5a)
607 indicate their derivation by high degree melting of mantle peridotite.

608 5.2.   Constraints from common Pb isotope data

609 Common Pb contained in mineral phases that strongly exclude U (e.g. K-feldspar,
610 galena) records the Pb isotopic composition of the source at the time of last
611 crystallization because there is no to negligible post-crystallization ingrowth of
612 radiogenic Pb. In $^{206}Pb/^{204}Pb$ vs. $^{208}Pb/^{204}Pb$ and $^{206}Pb/^{204}Pb$ vs. $^{207}Pb/^{204}Pb$
613 diagrams, Pb isotopic composition of the studied samples cluster closely around
614 the model Pb-evolution curve of Stacey and Kramers (1975) at ~3.3 Ga and ~3.1
615 Ga (Fig. 6). This narrow range of initial Pb-isotope ratios for rocks covering most of
616 the Singhbhum craton implies that the source of the granitoids was quite
617 homogenous and mantle-derived, and later metamorphic processes had no
618 discernible effect on the Pb-isotopes in feldspar. This attests to the absence of later
619 overprint that is common and extensive in other crustal terranes of the same age
620 like the contemporaneous Dharwar craton or the well-studied Barberton region,
621 which show extensive reworking during medium to high grade metamorphism and
622 magmatism in the late Archean and even the Proterozoic. The Pb isotope
623 compositions in K-feldspars from the West Greenland also show a much wider
624 range, indicating disturbance long after the formation of primary rock suite (Fig. 6).

625 Thus, the Pb isotopes provide strong support for the pristine character of granitoids

626 of the Singhbhum craton, where the last overprinting occurred before ca. 3.1 Ga;

627 making these rock suites suitable for isotopic studies that try to define the initial

628 conditions of crust formation. The Pb isotopes from these samples show no

629 evidence for the presence of much older crustal material with a high μ (i.e.

630 $^{238}U/^{204}Pb$). The high Pb concentrations in crustal material, and higher growth rate

631 of $^{207}Pb/^{204}Pb$ expected in older evolved crust would have resulted in Pb isotope

632 composition above the mantle growth curve in Fig. 6b. The close agreement of the

633 Pb isotopes from K-feldspars with the model mantle curve and the general absence

634 of older zircons attests to the juvenile character of these evolved rock suites and

635 the insignificance of Hadean or Eoarchean crustal material in these rocks or their

636 source.

637 5.3.   Nd-Hf isotopic constraints on crustal evolution of the Singhbhum craton

638 Most of the Paleoarchean granitoids of the Singhbhum craton have εNd_i values

639 (whole rock) ranging from -0.2 to +2.2 ($2\sigma = \sim 1\varepsilon$) indicating a chondritic to slightly

640 depleted source for these rocks (Fig. 10a). Taking the uncertainty on εNd_i values

641 ($2\sigma = \sim 1\varepsilon$) into account, these samples have a very restricted spread of εNd_i, with

642 values that are near-chondritic.

643 The mean in-situ εHf_i values for the zircon grains from the granitoids (3470-3263

644 Ma) range from -0.5±0.8 ($2\sigma_m$) to +2.1±0.6 ($2\sigma_m$) and are thus characteristic of a

645 chondritic to slightly depleted source (Table 5, Fig. 10b). The mean εHf_i values of

646 the studied granitoids overlap within uncertainties indicating a homogeneous

647 source. Dey et al. (2017) reported Hf isotope data for the 3.47, 3.35, and 3.30 Ga

648 granitoids (from the central part of the Singhbhum craton) having εHf_i values (in-situ

649 zircon) of +2.1±2.8 – +4.8±2.8 (2σ), +1.8±3.0 – +4.0±3.6 (2σ), and +0.8±2.8 –

650 +3.7±2.8 (2σ) respectively, which are in agreement (within uncertainty) with the Hf

651 data of this study.

652 Some samples with higher εNd_i values (e.g. Om 12, $\varepsilon Nd_{3470\ Ma}$ = +5.2) suggest a

653 strongly depleted mantle source; however, the low εHf_i values of the same samples

654 (e.g. Om 12, $\varepsilon Hf_{3470\ Ma}$ = +0.1±1.1) indicate a near-chondritic source (see section

655 4.5; Table 5). Since there is no existing model which could account for the

656 decoupling of Sm-Nd and Lu-Hf systems during magma evolution, the disparity

between high εNd_i (whole rock) and near-chondritic εHf_i values (in-situ zircon) for the samples Om 12, Om 11a, and Om 5b (Table 5) requires a post-magmatic decoupling of the Sm-Nd signature of the whole rock from the Lu-Hf signature in zircon grains, for example during metamorphic events (McCulloch and Black, 1984; Windrim et al., 1984; Black and McCulloch, 1987; Whitehouse, 1988; Bridgwater et al., 1989; Li et al., 1990; Tourpin et al., 1991; Gruau et al., 1992; Frost and Frost, 1995; Lahaye et al., 1995; Poitrasson et al., 1995; Gruau et al., 1996; Moorbath et al., 1997). Evidence for alteration is observed in the zircons of the samples Om 12, Om 11a, and Om 5b, as many of the zircons yielded very low $^{206}Pb/^{204}Pb$ (<50) which were then not included for age calculations. Even the zircons from these samples that yielded the concordant U-Pb ages have altered rims (Fig. 7). Since Hf isotopes (and U-Pb dates) reported here, were measured from the most intact domains of the zircon grains, their composition (near chondritic) should be the source signature. In contrast, the whole rock Nd isotope for the samples with largely altered zircons appear disturbed.

All zircons from the major units of the Singhbhum craton are younger than 3.5 Ga and older than 3.2 Ga, which means that major crust formation happened at that time from a near chondritic source. However, the rare Hadean-Eoarchean inherited and detrital zircons (4.24-3.61 Ga) reported from the Singhbhum craton (e.g. Upadhyay et al., 2014; Chaudhuri et al., 2018; Miller et al., 2018) suggest the formation of some crust in that time period. Chaudhuri et al. (2018) reported εHf_i values (SHRIMP in-situ zircon) of -2.5±1.6 to -5.2±1.3 for 4.24-4.03 Ga of xenocrystic zircons from OMTG. A single zircon (4.01 Ga) from the modern sediment of the Baitarani River within the Singhbhum craton yielded a εHf_i value (LA-MC-ICPMS in-situ zircon) of -5.3±4.1 (Miller et al., 2018). These negative (i.e. sub-chondritic) initial εHf values for the Hadean zircons indicate that they were formed from an enriched source (e.g. TTG magma). However, near-chondritic to slightly depleted Nd and Hf isotopic signatures for the Paleoarchean granitoids of the Singhbhum craton suggest that very limited volumes of crust formed and/or was recycled back into the mantle before emplacement of the Singhbhum granitoids. In addition, the homogeneous composition of the Pb isotopes (Table 3, Fig. 6) and the narrow range in initial Hf isotopes argue against the recycling of large amounts of crust into the source of the major rock units of the Singhbhum craton and are more consistent with a primitive near-chondritic source.

691   5.4.   Implications for the crustal evolution on the early Earth

692   Many Sm-Nd and Lu-Hf isotopic studies have been conducted on Hadean-Archean
693   terranes (e.g. West Greenland, Canadian Shield, Kaapvaal craton, and Yilgarn
694   craton) to reconstruct the evolution of the continental crust on the early Earth (Figs.
695   10c, d). Bennet et al. (1993) reported initial εNd values ranging from +4.5 to -4.5 for
696   3.87-3.76 Ga metadiorites and tonalities from southern West Greenland suggesting
697   extreme Nd-isotope heterogeneity in the early Archean. Similar data were reported
698   for the Acasta gneisses (zircon U-Pb age 4.0-3.6 Ga) with initial εNd values of -4.8
699   to +3.6 viewed as supporting a heterogeneous and depleted reservoir in the
700   Hadean-Eoarchean period (Fig. 10c) (Bowring and Housh, 1995). However, these
701   were contested by Moorbath et al. (1997) and Whitehouse (2001) who argued that
702   the initial εNd values calculated based on zircon U-Pb ages in these studies may
703   be of little or no significance for early crust-mantle geochemical evolution as those
704   rock suites have undergone later tectonometamorphic events which led to effective
705   resetting of the Sm-Nd system. Recent Hf isotope studies on zircons of the
706   Eoarchean rocks from West Greenland demonstrate a near chondritic source (εHf$_i$
707   = -1.3 to +1.0; Fig.10d) of these rocks (e.g. Kemp et al., 2009; Fisher and Vervoort,
708   2018). Hadean-Paleoarchean zircons from the Canadian Shield (Acasta gneisses)
709   show sub-chondritic to chondritic initial Hf isotopic compositions (εHf$_i$ = -9.6 to
710   +0.7), except for two 4.02 Ga zircons with εHf$_i$ of +2.7 and +3.4 (Fig. 10d) (e.g.
711   Iizuka et al., 2009; Reimink et al., 2016; Bauer et al., 2017). The sub-chondritic
712   initial Hf isotopic composition of the zircons from the Acasta gneisses essentially
713   indicate the formation of some felsic crust in the Hadean-Eoarchean, but a majority
714   of the data do not support the extremely depleted Nd signature as suggested by
715   Bennet et al. (1993) and Bowring and Housh (1995) (Figs. 10c, d).

716   Schoene et al. (2009) reported sub-chondritic to slightly depleted whole rock initial
717   εNd values (-4.6 to +1.6) for ca. 3.7-3.1 Ga granitoids of the Kaapvaal craton,
718   except a few outliers ranging from +2.8 to +6.4 (Fig. 10c). These outliers were
719   viewed as the result of local alteration and disturbance of Sm-Nd system (Schoene
720   et al., 2009). Zircon Hf isotope data from these rocks indicate an enriched to slightly
721   depleted source (εHf$_i$ = -6.8 to +2.2; Fig. 10d) (e.g. Zeh et al., 2011; Hoffmann et
722   al., 2016). Within uncertainties the majority of initial εHf data are (near) chondritic.
723   Nutman et al. (1993) reported whole rock Nd isotope data for ~3.7-3.1 Ga gneisses
724   and granites of Yilgarn craton (Western Australia) ranging from -3.9 to +2.4 (Fig.

725   10c). Most of the Hadean-Paleoarchean detrital zircon grains from the Jack Hills

726   and Mt. Narryer (Yilgarn craton, Western Australia) yield sub-chondritic (negative)

727   initial εHf values, except very few with positive values (Fig. 10d) (e.g. Kemp et al.,

728   2010; Nebel-Jacobsen, 2010).

729   Combining the initial Hf isotope compositions of most of the Eoarchean-

730   Paleoarchean zircons from major Eoarchean-Paleoarchean cratons (e.g. West

731   Greenland, Acasta gneisses, Yilgarn craton, Kaapvaal craton, and Singhbhum

732   craton) indicate their derivation from near-chondritic to slightly depleted reservoir

733   (Figs. 10c & d). They also confirm that extreme Nd depletion signatures found in

734   some studies are the results of disturbance in Sm/Nd ratios of the rocks after their

735   formation. Hence, extrapolation of the initial εNd to the zircon crystallization ages

736   yield strongly positive but inaccurate values. The subchondritic initial Hf isotopic

737   compositions of detrital zircons (Hadean to early Archean) from the Yilgarn craton

738   (Jack Hills and Mt. Narryer) and zircons from Acasta gneisses essentially confirm

739   the presence of felsic crust in the Hadean but they do not show strong evidence of

740   mantle depletion during that period. The literature reports of crust older than ca.

741   3.5 Ga pertain to limited rock volumes, most of which were either assimilated or

742   otherwise recycled.

743   If the mantle source for that generated the continental crust was still near chondritic

744   at ca. 3.5 Ga as suggested by the Hf and Nd data from the Singhbhum craton and

745   other Eoarchean-Paleoarchean terranes, then major depletion of the mantle and

746   concomitant crust formation started at ca. 3.5 Ga. Using this point in time for the

747   beginning of major crust formation and the present-day isotope composition of the

748   depleted mantle, i.e. the chemical complement to the enriched continental crust, Nd

749   and Hf depletion trends for the mantle can be derived in analogy to previous

750   models (e.g. DePaolo, 1981; Goldstein et al., 1984; Nägler and Kramers, 1998)

751   (Fig. 10a, b):

752   εNd_t = -2.78 x (t_{Ga}) + 10, and

753   εHf_t = -4.56 x (t_{Ga}) + 16.4.

754   These curves will not change the model ages for the young rocks significantly, but,

755   they will make a major difference for the old rocks (i.e. Archean). If these equations

756   describe the average depletion the mantle, they cannot be used to obtain model

757   ages with geological significance for Paelo- and Eoarchean rocks.

6. Conclusions

759   The East Singhbhum Volcanic Rocks are basalt to basaltic andesite, whereas the

760   West Singhbhum Volcanic Rocks are more evolved and range from basaltic

761   andesitic to andesitic composition. The East Singhbhum Volcanic Rocks and East

762   Singhbhum Komatiites have flat REE patterns, no significant Eu anomaly, and a

763   negative K anomaly; whereas the West Singhbhum Volcanic Rocks have slightly

764   fractionated REE pattern with negative Eu anomaly, and positive K and Pb

765   anomalies. This indicates their derivation from two distinct sources. The high Ni and

766   Cr contents of the East Singhbhum Volcanic Rocks (Ni = 240-800 ppm, Cr = 760-

767   2520 ppm) and East Singhbhum Komatiite (Ni = 1680-2070 ppm, Cr = 1240-1680

768   ppm) and almost flat REE patterns indicate their derivation by high degree melting

769   of mantle peridotite. The West Singhbhum Volcanic Rocks with mantle like Cr (330-

770   1380 ppm) and Ni (130-460 ppm) contents attest to their derivation from primitive

771   mantle derived melts. Therefore, their positive K and Pb anomalies, which are also

772   observed in the granitoids, are a mantle signature. This indicates that the source of

773   the older granitoids share chemical similarities with the source of the younger

774   volcanic rocks in the craton.

775   The Paleoarchean granitoids of the Singhbhum craton formed between ca. 3.5 and

776   3.2 Ga by partial melting of a basaltic-andesitic crust at variable depths

777   corresponding to ca. 10-15 kbar. The Pb, Hf and Nd isotope compositions of these

778   rocks indicate an origin from a near-chondritic reservoir, meaning that the mantle

779   source of the Singhbhum granitoids was not significantly depleted and possibly only

780   a small volume of enriched continental crust had been extracted from the mantle by

781   this time. The Pb isotopes from leached K-feldspars are mantle like and indicate

782   that only insignificant amounts of older crust contributed to the igneous rocks of the

783   craton either in the source or through assimilation. Besides rare older zircon grains,

784   the rocks do not show evidence for the presence of older enriched crustal material.

785   The formation of the Singhbhum craton at ca. 3.5-3.2 Ga coincides with the

786   appearance of the first extensive continental crust worldwide as observed in other

787   cratons (e.g. Kaapvaal, Yilgarn, Dharwar, and Bastar). This may indicate the onset

788   of significant growth of continental crust and concomitant mantle depletion.

789

799

References

Acharyya, S.K., Gupta, A. and Orihashi, Y., 2010. New U-Pb zircon ages from Paleo-Mesoarchean TTG gneisses of the Singhbhum Craton, eastern India. Geochemical Journal, 44, 81-88.

Armstrong, R.A., Compston, W., De Wit, M.J. and Williams, I.S., 1990. The stratigraphy of the 3.5-3.2 Ga Barberton Greenstone Belt revisited: a single zircon ion microprobe study. Earth and Planetary Science Letters, 101, 90-106.

Armstrong, R.L., 1991. The persistent myth of crustal growth. Australian Journal of Earth Sciences, 38, 613-630.

Baadsgaard, H., 1976. Further U-Pb dates on zircons from the early Precambrian rocks of the Godthaabsfjord area, West Greenland. Earth and Planetary Science Letters, 33, 261-267.

Barker, F., 1979. Trondhjemite: definition, environment and hypotheses of origin. In: Barker, F. (Ed.), Trondhjemite, Dacite and Related Rocks. Elsevier, Amsterdam, 1-12.

Basu, A.R., Sharma, M., Premo, W.R., 1993. U–Pb age of an older metamorphic group mica schist: earliest terrain of the eastern Indian craton. In: Saha, A.K. (Ed.), Recent Researches in Geology and Geophysics of the Precambrians. Recent Researches in Geology, 16, 93–102.

818 Bauer, A.M., Fisher, C.M., Vervoort, J.D. and Bowring, S.A., 2017. Coupled zircon Lu–
819 Hf and U–Pb isotopic analyses of the oldest terrestrial crust, the >4.03 Ga Acasta
820 Gneiss Complex. Earth and Planetary Science Letters, 458, 37-48.

821 Belousova, E.A., Kostitsyn, Y.A., Griffin, W.L., Begg, G.C., O'Reilly, S.Y. and Pearson,
822 N.J., 2010. The growth of the continental crust: constraints from zircon Hf-isotope data.
823 Lithos, 119, 457-466.

824 Bennett, V.C., Nutman, A.P. and McCulloch, M.T., 1993. Nd isotopic evidence for
825 transient, highly depleted mantle reservoirs in the early history of the Earth. Earth and
826 Planetary Science Letters, 119, 299-317.

827 Black, L.P. and McCulloch, M.T., 1987. Evidence for isotopic equilibration of Sm-Nd
828 whole-rock systems in early Archaean crust of Enderby Land, Antarctica. Earth and
829 Planetary Science Letters, 82, 15-24.

830 Black, L.P., Gale, N.H., Moorbath, S., Pankhurst, R.J. and McGregor, V.R., 1971.
831 Isotopic dating of very early Precambrian amphibolite facies gneisses from the
832 Godthaab district, West Greenland. Earth and Planetary Science Letters, 12, 245-259.

833 Black, L.P., Kamo, S.L., Allen, C.M., Davis, D.W., Aleinikoff, J.N., Valley, J.W., Mundil,
834 R., Campbell, I.H., Korsch, R.J., Williams, I.S. and Foudoulis, C., 2004. Improved
835 $^{206}Pb/^{238}U$ microprobe geochronology by the monitoring of a trace-element-related
836 matrix effect; SHRIMP, ID–TIMS, ELA–ICP–MS and oxygen isotope documentation for
837 a series of zircon standards. Chemical Geology, 205, 115-140.

838 Blichert-Toft, J. and Albarède, F., 1997. The Lu-Hf isotope geochemistry of chondrites
839 and the evolution of the mantle-crust system. Earth and Planetary Science Letters,
840 148, 243-258.

841 Blichert-Toft, J. and Albarède, F., 2008. Hafnium isotopes in Jack Hills zircons and the
842 formation of the Hadean crust. Earth and Planetary Science Letters, 265, 686-702.

843 Bouvier, A., Vervoort, J.D. and Patchett, P.J., 2008. The Lu–Hf and Sm–Nd isotopic
844 composition of CHUR: constraints from unequilibrated chondrites and implications for
845 the bulk composition of terrestrial planets. Earth and Planetary Science Letters, 273,
846 48-57.

847 Bowring, S.A. and Housh, T., 1995. The Earth's early evolution. Science, 269, 1535-
848 1540.

849 Bridgwater, D., Rosing, M. and Schiotte, L., 1989. The effect of fluid-controlled element
850 mobility during metamorphism on whole rock isotope systems, some theoretical
851 aspects and possible examples. In: D. Bridgwater (Editor), Fluid Movements - Element
852 Transport and the Composition of the Deep Crust. Kluwer, Amsterdam, 277-298.

853 Chaudhuri, T., Mazumder, R., Arima, M., 2015. Petrography and geochemistry of
854 Mesoarchaean komatiites from the eastern Iron Ore belt, Singhbhum craton, India, and
855 its similarity with 'Barberton type komatiite'. Journal of African Earth Sciences, 101,
856 135-147.

857 Chaudhuri, T., Satish-Kumar, M., Mazumder, R. and Biswas, S., 2017. Geochemistry
858 and Sm-Nd isotopic characteristics of the Paleoarchean Komatiites from Singhbhum
859 Craton, Eastern India and their implications. Precambrian Research, 298, 385-402.

860 Chaudhuri, T., Wan, Y., Mazumder, R., Ma, M. and Liu, D., 2018. Evidence of
861 Enriched, Hadean Mantle Reservoir from 4.2-4.0 Ga zircon xenocrysts from
862 Paleoarchean TTGs of the Singhbhum Craton, Eastern India. Scientific reports, 8,
863 7069.

864 Chu, N.C., Taylor, R.N., Chavagnac, V., Nesbitt, R.W., Boella, R.M., Milton, J.A.,
865 German, C.R., Bayon, G. and Burton, K., 2002. Hf isotope ratio analysis using multi-
866 collector inductively coupled plasma mass spectrometry: an evaluation of isobaric
867 interference corrections. Journal of Analytical Atomic Spectrometry, 17, 1567-1574.

868 Compston, W., Kinny, P.D., Williams, I.S. and Foster, J.J., 1986. The age and Pb loss
869 behaviour of zircons from the Isua supracrustal belt as determined by ion microprobe.
870 Earth and Planetary Science Letters, 80, 71-81.

871 Condie, K.C., 1998. Episodic continental growth and supercontinents: a mantle
872 avalanche connection? Earth and Planetary Science Letters, 163, 97-108.

873 Condie, K.C., 2000. Episodic continental growth models: afterthoughts and extensions.
874 Tectonophysics, 322, 153-162.

875 de Wit, M.J., Armstrong, R., Hart, R.J. and Wilson, A.H., 1987. Felsic igneous rocks
876 within the 3.3 to 3.5-Ga Barberton Greenstone Belt: High crustal level equivalents of

877 the surrounding Tonalite-Trondhjemite Terrain, emplaced during thrusting. Tectonics,
878 6, 529-549.

879 DePaolo, D.J. and Wasserburg, G.J., 1976a. Nd isotopic variations and petrogenetic
880 models. Geophysical Research Letters, 3, 249-252.

881 DePaolo, D.J. and Wasserburg, G.J., 1976b. Inferences about magma sources and
882 mantle structure from variations of $^{143}Nd/^{144}Nd$. Geophysical Research Letters, 3, 743-
883 746.

884 DePaolo, D.J., 1981. A neodymium and strontium isotopic study of the Mesozoic
885 calc-alkaline granitic batholiths of the Sierra Nevada and Peninsular Ranges,
886 California. Journal of Geophysical Research: Solid Earth, 86, 10470-10488.

887 Devaraju, T.C., Huhma, H., Sudhakara, T.L., Kaukonen, R.J. and Alapieti, T.T., 2007.
888 Petrology, geochemistry, model Sm-Nd ages and petrogenesis of the granitoids of the
889 northern block of Western Dharwar Craton. . Journal of the Geological Society of India,
890 70, 889-911.

891 Dey, S., 2013. Evolution of Archaean crust in the Dharwar craton: the Nd isotope
892 record. Precambrian Research, 227, 227-246.

893 Dey, S., Topno, A., Liu, Y. and Zong, K., 2017. Generation and evolution of
894 Palaeoarchaean continental crust in the central part of the Singhbhum craton, eastern
895 India. Precambrian Research, 298, 268-291.

896 Fisher, C.M. and Vervoort, J.D., 2018. Using the magmatic record to constrain the
897 growth of continental crust-The Eoarchean zircon Hf record of Greenland. Earth and
898 Planetary Science Letters, 488, 79-91.

899 Fisher, C.M., Vervoort, J.D. and Hanchar, J.M., 2014. Guidelines for reporting zircon Hf
900 isotopic data by LA-MC-ICPMS and potential pitfalls in the interpretation of these data.
901 Chemical Geology, 363, 125-133.

902 Frost, C.D. and Frost, B.R., 1995. Open-system dehydration of amphibolite, Morton
903 Pass, Wyoming: Elemental and Nd and Sr isotopic effects. The Journal of Geology,
904 103, 269-284.

905 Ghosh, J.G., 2004. 3.56 Ga tonalite in the central part of the Bastar craton, India:
906 oldest Indian date. Journal of Asian Earth Sciences, 23, 359-364.

907 Goldstein, S.L., O'nions, R.K. and Hamilton, P.J., 1984. A Sm-Nd isotopic study of
908 atmospheric dusts and particulates from major river systems. Earth and planetary
909 Science Letters, 70, 221-236.

910 Goswami, J.N., Mishra, S., Wiedenbeck, M., Ray, S.L. and Saha, A.K., 1995. 3.55 Ga
911 old zircon from Singhbhum-Orissa iron ore craton, eastern India. Current Science, 69,
912 1008-1012.

913 Gruau, G., Rosing, M., Bridgwater, D. and Gill, R.C.O., 1996. Resetting of Sm-Nd
914 systematics during metamorphism of >3.7-Ga rocks: implications for isotopic models of
915 early Earth differentiation. Chemical Geology, 133, 225-240.

916 Gruau, G., Tourpin, S., Fourcade, S. and Blais, S., 1992. Loss of isotopic (Nd, O) and
917 chemical (REE) memory during metamorphism of komatiites: new evidence from
918 eastern Finland. Contributions to Mineralogy and Petrology, 112, 66-82.

919 Harrison, T.M., Blichert-Toft, J., Müller, W., Albarède, F., Holden, P. and Mojzsis, S.J.,
920 2005. Heterogeneous Hadean hafnium: evidence of continental crust at 4.4 to 4.5 Ga.
921 Science, 310, 1947-1950.

922 Hoffmann, J.E., Kröner, A., Hegner, E., Viehmann, S., Xie, H., Iaccheri, L.M.,
923 Schneider, K.P., Hofmann, A., Wong, J., Geng, H. and Yang, J., 2016. Source
924 composition, fractional crystallization and magma mixing processes in the 3.48-3.43 Ga
925 Tsawela tonalite suite (Ancient Gneiss Complex, Swaziland)-implications for
926 Palaeoarchaean geodynamics. Precambrian Research, 276, 43-66.

927 Hoffmann, J.E., Münker, C., Næraa, T., Rosing, M.T., Herwartz, D., Garbe-Schönberg,
928 D. and Svahnberg, H., 2011. Mechanisms of Archean crust formation inferred from
929 high-precision HFSE systematics in TTGs. Geochimica et Cosmochimica Acta, 75,
930 4157-4178.

931 Hofmann, A. and Mazumder, R., 2015. A review of the current status of the Older
932 Metamorphic Group and Older Metamorphic Tonalite Gneiss: insights into the
933 Palaeoarchaean history of the Singhbhum craton, India. Geological Society, London,
934 Memoirs, 43, 103-107.

935 Hurley, P.M. and Rand, J.R., 1969. Pre-drift continental nuclei. Science, 164, 1229-
936 1242.

937 Ickert, R.B., 2013. Algorithms for estimating uncertainties in initial radiogenic isotope
938 ratios and model ages. Chemical Geology, 340, 131-138.

939 Iizuka, T., Komiya, T., Johnson, S.P., Kon, Y., Maruyama, S. and Hirata, T., 2009.
940 Reworking of Hadean crust in the Acasta gneisses, northwestern Canada: evidence
941 from in-situ Lu–Hf isotope analysis of zircon. Chemical Geology, 259, 230-239.

942 Jackson, S.E., Pearson, N.J., Griffin, W.L. and Belousova, E.A., 2004. The application
943 of laser ablation-inductively coupled plasma-mass spectrometry to in situ U–Pb zircon
944 geochronology. Chemical Geology, 211, 47-69.

945 Jacobsen, S.B. and Wasserburg, G.J., 1980. Sm-Nd isotopic evolution of chondrites.
946 Earth and Planetary Science Letters, 50, 139-155.

947 Kamber, B.S. and Moorbath, S., 1998. Initial Pb of the Amitsoq gneiss revisited:
948 implication for the timing of early Archaean crustal evolution in West Greenland.
949 Chemical Geology, 150, 19-41.

950 Kamber, B.S., Collerson, K.D., Moorbath, S. and Whitehouse, M.J., 2003. Inheritance
951 of early Archaean Pb-isotope variability from long-lived Hadean protocrust.
952 Contributions to Mineralogy and Petrology, 145, 25-46.

953 Kamo, S.L. and Davis, D.W., 1994. Reassessment of Archean crustal development in
954 the Barberton Mountain Land, South Africa, based on U-Pb dating. Tectonics, 13, 167-
955 192.

956 Kaur, P., Zeh, A. and Chaudhri, N., 2014. Characterisation and U–Pb–Hf isotope
957 record of the 3.55 Ga felsic crust from the Bundelkhand Craton, northern India.
958 Precambrian Research, 255, 236-244.

959 Kemp, A.I.S., Foster, G.L., Scherstén, A., Whitehouse, M.J., Darling, J. and Storey, C.,
960 2009. Concurrent Pb–Hf isotope analysis of zircon by laser ablation multi-collector ICP-
961 MS, with implications for the crustal evolution of Greenland and the Himalayas.
962 Chemical Geology, 261, 244-260.

963 Kemp, A.I.S., Hawkesworth, C.J., Paterson, B.A. and Kinny, P.D., 2006. Episodic
964 growth of the Gondwana supercontinent from hafnium and oxygen isotopes in zircon.
965 Nature, 439, 580-583.

966 Kemp, A.I.S., Wilde, S.A., Hawkesworth, C.J., Coath, C.D., Nemchin, A., Pidgeon,
967 R.T., Vervoort, J.D. and DuFrane, S.A., 2010. Hadean crustal evolution revisited: new
968 constraints from Pb–Hf isotope systematics of the Jack Hills zircons. Earth and
969 Planetary Science Letters, 296, 45-56.

970 Korenaga, J., 2013. Initiation and evolution of plate tectonics on Earth: theories and
971 observations. Annual Review of Earth and Planetary Sciences, 41, 117-151.

972 Kramers, J.D. and Tolstikhin, I.N., 1997. Two terrestrial lead isotope paradoxes,
973 forward transport modelling, core formation and the history of the continental crust.
974 Chemical Geology, 139, 75-110.

975 Kröner, A. and Todt, W., 1988. Single zircon dating constraining the maximum age of
976 the Barberton greenstone belt, southern Africa. Journal of Geophysical Research: Solid
977 Earth, 93, 15329-15337.

978 Kröner, A., Anhaeusser, C.R., Hoffmann, J.E., Wong, J., Geng, H., Hegner, E., Xie, H.,
979 Yang, J. and Liu, D., 2016. Chronology of the oldest supracrustal sequences in the
980 Palaeoarchaean Barberton Greenstone Belt, South Africa and Swaziland. Precambrian
981 Research, 279, 123-143.

982 Kröner, A., Hegner, E., Wendt, J.I. and Byerly, G.R., 1996. The oldest part of the
983 Barberton granitoid-greenstone terrain, South Africa: evidence for crust formation
984 between 3.5 and 3.7 Ga. Precambrian Research, 78, 105-124.

985 Lahaye, Y., Arndt, N., Byerly, G., Chauvel, C., Fourcade, S. and Gruau, G., 1995. The
986 influence of alteration on the trace-element and Nd isotopic compositions of komatiites.
987 Chemical Geology, 126, 43-64.

988 Le Maitre, R.W., Bateman, P., Dudek, A., Keller, J., Lameyre, J., Le Bas, M.J., Sabine,
989 P.A., Schmid, R., Sorensen, H., Streckeisen, A., Woolley, A.R. & Zanettin, B., 1989: A
990 Classification of Igneous Rocks and Glossary of Terms: Recommendations of the
991 International Union of Geological Sciences Subcommission on the Systematics of
992 Igneous Rocks. Blackwell Scientific Publications, Oxford.

993 Li, S., Hart, S.R. and Wu, T., 1990. Rb-Sr and Sm-Nd isotopic dating of an early
994 Precambrian spilite-keratophyre sequence in the Wutaishan area, North China:
995 preliminary evidence for Nd-isotopic homogenization in the mafic and felsic lavas
996 during low-grade metamorphism. Precambrian Research, 47, 191-203.

997   Liu, D., Wilde, S.A., Wan, Y., Wu, J., Zhou, H., Dong, C. and Yin, X., 2008. New U-Pb
998   and Hf isotopic data confirm Anshan as the oldest preserved segment of the North
999   China Craton. American Journal of Science, 308, 200-231.

1000   Liu, D.Y., Nutman, A.P., Compston, W., Wu, J.S. and Shen, Q.H., 1992. Remnants of
1001   ≥3800 Ma crust in the Chinese part of the Sino-Korean craton. Geology, 20, 339-342.

1002   Ludwig, K.R., 2003. User's Manual for ISOPLOT 3.00: A Geochronological Toolkit for
1003   Microsoft Excel, Special Publication No. 4. Berkeley Geochronology Center, 1-70.

1004   McCulloch, M.T. and Bennett, V.C., 1994. Progressive growth of the Earth's continental
1005   crust and depleted mantle: geochemical constraints. Geochimica et Cosmochimica
1006   Acta, 58, 4717-4738.

1007   McCulloch, M.T. and Black, L.P., 1984. Sm-Nd isotopic systematics of Enderby Land
1008   granulites and evidence for the redistribution of Sm and Nd during metamorphism.
1009   Earth and Planetary Science Letters, 71, 46-58.

1010   Miller, S.R., Mueller, P.A., Meert, J.G., Kamenov, G.D., Pivarunas, A.F., Sinha, A.K.,
1011   Pandit, M.K., 2018. Detrital Zircons Reveal Evidence of Hadean Crust in the
1012   Singhbhum Craton, India. The Journal of Geology, 126, 541-552.

1013   Mishra, S., Deomurari, M.P., Wiedenbeck, M., Goswami, J.N., Ray, S. and Saha, A.K.,
1014   1999. $^{207}Pb/^{206}Pb$ zircon ages and the evolution of the Singhbhum Craton, eastern
1015   India: an ion microprobe study. Precambrian Research, 93, 139-151.

1016   Misra, S., 2006. Precambrian chronostratigraphic growth of Singhbhum-Orissa craton,
1017   Eastern Indian shield: an alternative model. Journal of the Geological Society of India,
1018   67, 356-378.

1019   Moorbath, S., O'nions, R.K., Pankhurst, R.J., Gale, N.H. and McGregor, V.R., 1972.
1020   Further rubidium-strontium age determinations on the very early Precambrian rocks of
1021   the Godthaab district, West Greenland. Nature Physical Science, 240, 78-82.

1022   Moorbath, S., Whitehouse, M.J. and Kamber, B.S., 1997. Extreme Nd-isotope
1023   heterogeneity in the early Archaean—fact or fiction? Case histories from northern
1024   Canada and West Greenland. Chemical Geology, 135, 213-231.

1025   Moyen, J.F. and Martin, H., 2012. Forty years of TTG research. Lithos, 148, 312-336.

1026 Moyen, J.F., 2011. The composite Archaean grey gneisses: petrological significance, 1027 and evidence for a non-unique tectonic setting for Archaean crustal growth. Lithos, 1028 123, 21-36.

1029 Mukhopadhyay, D., 2001. The Archaean nucleus of Singhbhum: the present state of 1030 knowledge. Gondwana Research, 4, 307-318.

1031 Mukhopadhyay, J., Beukes, N.J., Armstrong, R.A., Zimmermann, U., Ghosh, G., 1032 Medda, R.A., 2008. Dating the oldest Greenstone in India, a 3.51 Ga precise U–Pb 1033 SHRIMP zircon age for Dacitic Lava of the Southern Iron Ore Group, Singhbhum 1034 Craton. The Journal of Geology, 116, 449-461.

1035 Myers, J.S., 1988. Early Archaean Narryer Gneiss Complex, Yilgarn Craton, Western 1036 Australia. Precambrian Research, 38, 297-307.

1037 Nägler, T.F. and Kramers, J.D., 1998. Nd isotopic evolution of the upper mantle during 1038 the Precambrian: models, data and the uncertainty of both. Precambrian Research, 91, 1039 233-252.

1040 Nebel-Jacobsen, Y., Münker, C., Nebel, O., Gerdes, A., Mezger, K. and Nelson, D.R., 1041 2010. Reworking of Earth's first crust: constraints from Hf isotopes in Archean zircons 1042 from Mt. Narryer, Australia. Precambrian Research, 182, 175-186.

1043 Nelson, D.R., Bhattacharya, H.N., Thern, E.R. and Altermann, W., 2014. Geochemical 1044 and ion-microprobe U–Pb zircon constraints on the Archaean evolution of Singhbhum 1045 Craton, eastern India. Precambrian Research, 255, 412-432.

1046 Nutman, A.P., Bennett, V.C., Friend, C.R. and Norman, M.D., 1999. Meta-igneous 1047 (non-gneissic) tonalites and quartz-diorites from an extensive ca. 3800 Ma terrain south 1048 of the Isua supracrustal belt, southern West Greenland: constraints on early crust 1049 formation. Contributions to Mineralogy and Petrology, 137, 364-388.

1050 Nutman, A.P., Bennett, V.C., Kinny, P.D. and Price, R., 1993. Large-scale crustal 1051 structure of the Northwestern Yilgarn Craton, western Australia: Evidence from Nd 1052 isotopic data and zircon geochronology. Tectonics, 12, 971-981.

1053 O'Neil, J., Carlson, R.W., Francis, D. and Stevenson, R.K., 2008. Neodymium-142 1054 evidence for Hadean mafic crust. Science, 321, 1828-1831.

O'Neil, J., Rizo, H., Boyet, M., Carlson, R.W. and Rosing, M.T., 2016. Geochemistry and Nd isotopic characteristics of Earth's Hadean mantle and primitive crust. Earth and Planetary Science Letters, 442, 194-205.

Patchett, P.J., Kouvo, O., Hedge, C.E. and Tatsumoto, M., 1981. Evolution of continental crust and mantle heterogeneity: evidence from Hf isotopes. Contributions to Mineralogy and Petrology, 78, 279-297.

Paul, D.K., Mukhopadhyay, D., Pyne, T.K., Bishoi, P.K., 1991. Rb–Sr age of granitoid in the Deo River section, Singhbhum and its relevance to the age of iron formation. Indian Minerals, 34, 51-56.

Pidgeon, R.T. and Wilde, S.A., 1990. The distribution of 3.0 Ga and 2.7 Ga volcanic episodes in the Yilgarn Craton of Western Australia. Precambrian Research, 48, 309-325.

Pidgeon, R.T., Macambira, M.J.B. and Lafon, J.M., 2000. Th–U–Pb isotopic systems and internal structures of complex zircons from an enderbite from the Pium Complex, Carajás Province, Brazil: evidence for the ages of granulite facies metamorphism and the protolith of the enderbite. Chemical Geology, 166, 159-171.

Poitrasson, F., Pin, C. and Duthou, J.L., 1995. Hydrothermal remobilization of rare earth elements and its effect on Nd isotopes in rhyolite and granite. Earth and Planetary Science Letters, 130, 1-11.

Ray, S.L., Saha, A.K. and Ghosh, S., 1987. Nature of the oldest known metasediments from eastern India. Indian Minerals, 41, 52-60.

Reimink, J.R., Davies, J.H.F.L., Chacko, T., Stern, R.A., Heaman, L.M., Sarkar, C., Schaltegger, U., Creaser, R.A. and Pearson, D.G., 2016. No evidence for Hadean continental crust within Earth's oldest evolved rock unit. Nature Geoscience, 9, 777-780.

Rino, S., Komiya, T., Windley, B.F., Katayama, I., Motoki, A. and Hirata, T., 2004. Major episodic increases of continental crustal growth determined from zircon ages of river sands; implications for mantle overturns in the Early Precambrian. Physics of the Earth and Planetary Interiors, 146, 369-394.

1084 Rollinson, H., 2008. Secular evolution of the continental crust: Implications for crust
1085 evolution models. Geochemistry, Geophysics, Geosystems, 9, 1-14.

1086 Rosas, J.C. and Korenaga, J., 2018. Rapid crustal growth and efficient crustal recycling
1087 in the early Earth: Implications for Hadean and Archean geodynamics. Earth and
1088 Planetary Science Letters, 494, 42-49.

1089 Saha, A.K., 1994. Crustal evolution of Singhbhum-North Orissa, Eastern India.
1090 Geological Society of India, Memoir 27, 341pp.

1091 Sahu, N.K., Mukherjee, M.M., 2001. Spinifex textured komatiite from Badampahar-
1092 Gorumahisani schist belt, Mayurbhanj District, Orissa. Journal of the Geological
1093 Society of India, 57, 529-534.

1094 Santos, J.O.S., Hartmann, L.A., Gaudette, H.E., Groves, D.I., Mcnaughton, N.J. and
1095 Fletcher, I.R., 2000. A new understanding of the provinces of the Amazon Craton
1096 based on integration of field mapping and U-Pb and Sm-Nd geochronology. Gondwana
1097 Research, 3, 453-488.

1098 Scherer, E., Münker, C. and Mezger, K., 2001. Calibration of the lutetium-hafnium
1099 clock. Science, 293, 683-687.

1100 Scherer, E.E., Whitehouse, M.J. and Munker, C., 2007. Zircon as a monitor of crustal
1101 growth. Elements, 3, 19-24.

1102 Schoene, B., Dudas, F.O., Bowring, S.A. and De Wit, M., 2009. Sm–Nd isotopic
1103 mapping of lithospheric growth and stabilization in the eastern Kaapvaal craton. Terra
1104 Nova, 21, 219-228.

1105 Sinha, A.K. and Tilton, G.R., 1973. Isotopic evolution of common lead. Geochimica et
1106 Cosmochimica Acta, 37, 1823-1849.

1107 Sláma, J., Košler, J., Condon, D.J., Crowley, J.L., Gerdes, A., Hanchar, J.M.,
1108 Horstwood, M.S., Morris, G.A., Nasdala, L., Norberg, N. and Schaltegger, U., 2008.
1109 Plešovice zircon—a new natural reference material for U–Pb and Hf isotopic
1110 microanalysis. Chemical Geology, 249, 1-35.

1111 Söderlund, U., Patchett, P.J., Vervoort, J.D. and Isaehsen, C.E., 2004. The [176]Lu decay
1112 constant determined by Lu-Hf and U-Pb isotope systematics of Precambrian mafic
1113 intrusions. Earth and Planetary Science Letters, 219, 311-324.

Stacey, J.T. and Kramers, J.D., 1975. Approximation of terrestrial lead isotope evolution by a two-stage model. Earth and Planetary Science Letters, 26, 207-221.

Stern, R.A. and Bleeker, W., 1998. Age of the world's oldest rocks refined using Canada's SHRIMP: the Acasta Gneiss Complex, Northwest Territories, Canada. Geoscience Canada, 25, 27-31.

Stracke, A., Scherer, E.E., Reynolds, B.C., 2014. 15.4 –Application of Isotope Dilution in Geochemistry. In: Heinrich, D., Turekian, K.K. (eds) Treatise on Geochemistry (Second Edition): Oxford, Elsevier, 71-86.

Sun, S.S. and McDonough, W.S., 1989. Chemical and isotopic systematics of oceanic basalts: implications for mantle composition and processes. Geological Society, London, Special Publications, 42, 313-345.

Tait, J., Zimmermann, U., Miyazaki, T., Presnyakov, S., Chang, Q., Mukhopadhyay, J. and Sergeev, S., 2011. Possible juvenile Palaeoarchaean TTG magmatism in eastern India and its constraints for the evolution of the Singhbhum craton. Geological Magazine, 148, 340-347.

Tanaka, T., Togashi, S., Kamioka, H., Amakawa, H., Kagami, H., Hamamoto, T., Yuhara, M., Orihashi, Y., Yoneda, S., Shimizu, H. and Kunimaru, T., 2000. JNdi-1: a neodymium isotopic reference in consistency with LaJolla neodymium. Chemical Geology, 168, 279-281.

Taylor, S.R. and McLennan, S.M., 1995. The geochemical evolution of the continental crust. Reviews of Geophysics, 33, 241-265.

Thirlwall, M.F. and Anczkiewicz, R., 2004. Multidynamic isotope ratio analysis using MC–ICP–MS and the causes of secular drift in Hf, Nd and Pb isotope ratios. International Journal of Mass Spectrometry, 235, 59-81.

Tolstikhin, I.N., Kramers, J.D. and Hofmann, A.W., 2006. A chemical Earth model with whole mantle convection: the importance of a core–mantle boundary layer (D ″) and its early formation. Chemical Geology, 226, 79-99.

Tourpin, S., Gruau, G., Blais, S. and Fourcade, S., 1991. Resetting of REE, and Nd and Sr isotopes during carbonitization of a komatiite flow from Finland. Chemical Geology, 90, 15-29.

1144 Ulrych, T.J., Burger, A. and Nicolaysen, L.O., 1967. Least radiogenic terrestrial leads.
1145 Earth and Planetary Science Letters, 2, 179-184.

1146 Upadhyay, D., Chattopadhyay, S., Kooijman, E., Mezger, K. and Berndt, J., 2014.
1147 Magmatic and metamorphic history of Paleoarchean tonalite–trondhjemite–granodiorite
1148 (TTG) suite from the Singhbhum craton, eastern India. Precambrian Research, 252,
1149 180-190.

1150 Vervoort, J.D., Patchett, P.J., Gehrels, G.E. and Nutman, A.P., 1996. Constraints on
1151 early Earth differentiation from hafnium and neodymium isotopes. Nature, 379, 624-
1152 627.

1153 Villa, I.M. and Hanchar, J.M., 2013. K-feldspar hygrochronology. Geochimica et
1154 Cosmochimica Acta, 101, 24-33.

1155 Villa, I.M., Ruggieri, G., Puxeddu, M. and Bertini, G., 2006. Geochronology and isotope
1156 transport systematics in a subsurface granite from the Larderello–Travale geothermal
1157 system (Italy). Journal of Volcanology and Geothermal Research, 152, 20-50.

1158 Whitehouse, M.J., 1988. Granulite fades Nd-isotopic homogenization in the Lewisian
1159 complex of northwest Scotland. Nature, 331, 705-707.

1160 Whitehouse, M.J., Nagler, T.F., Moorbath, S., Kramers, J.D., Kamber, B.S. and Frei,
1161 R., 2001. Priscoan (4.00-4.03 Ga) orthogneisses from northwestern Canada-by
1162 Samuel A. Bowring and Ian S. Williams: discussion. Contributions to Mineralogy and
1163 Petrology, 141, 248-250.

1164 Whitney, D.L. and Evans, B.W., 2010. Abbreviations for names of rock-forming
1165 minerals. American Mineralogist, 95, 185-187.

1166 Wiedenbeck, M.A.P.C., Alle, P., Corfu, F., Griffin, W.L., Meier, M., Oberli, F.V., Quadt,
1167 A.V., Roddick, J.C. and Spiegel, W., 1995. Three natural zircon standards for U-Th-Pb,
1168 Lu-Hf, trace element and REE analyses. Geostandards Newsletter, 19, 1-23.

1169 Wilde, S.A., Valley, J.W., Peck, W.H. and Graham, C.M., 2001. Evidence from detrital
1170 zircons for the existence of continental crust and oceans on the Earth 4.4 Gyr ago.
1171 Nature, 409, 175-178.

1172   Wilson, A.H. and Carlson, R.W., 1989. A Sm-Nd and Pb isotope study of Archaean
1173   greenstone belts in the southern Kaapvaal Craton, South Africa. Earth and Planetary
1174   Science Letters, 96, 89-105.

1175   Windrim, D.P., McCulloch, M.T., Chappell, B.W. and Cameron, W.E., 1984. Nd isotopic
1176   systematics and chemistry of Central Australian sapphirine granulites: an example of
1177   rare earth element mobility. Earth and Planetary Science Letters, 70, 27-39.

1178   Yadav, P.K., Pradhan, U.K., Mukherjee, A., Sar, R.N., Sahoo, P., Das, M., 2015. Basic
1179   characterization of Kapili komatiite from Badampahar-Gorumahishani schist belt,
1180   Singhbhum Craton, Odisha, India. Indian Journal of Geosciences, 69, 1–12.

1181   Zeh, A., Gerdes, A. and Heubeck, C., 2013. U–Pb and Hf isotope data of detrital
1182   zircons from the Barberton Greenstone Belt: constraints on provenance and Archaean
1183   crustal evolution. Journal of the Geological Society, 170, 215-223.

1184   Zeh, A., Gerdes, A. and Millonig, L., 2011. Hafnium isotope record of the Ancient
1185   Gneiss Complex, Swaziland, southern Africa: evidence for Archaean crust–mantle
1186   formation and crust reworking between 3.66 and 2.73 Ga. Journal of the Geological
1187   Society, 168, 953-964.

1188   Zeh, A., Gerdes, A., Klemd, R. and Barton Jr, J.M., 2007. Archaean to Proterozoic
1189   crustal evolution in the central zone of the Limpopo Belt (South Africa–Botswana):
1190   constraints from combined U–Pb and Lu–Hf isotope analyses of zircon. Journal of
1191   Petrology, 48, 1605-1639.

1192   Zeh, A., Gerdes, A., Klemd, R. and Barton Jr, J.M., 2008. U–Pb and Lu–Hf isotope
1193   record of detrital zircon grains from the Limpopo Belt–evidence for crustal recycling at
1194   the Hadean to early-Archean transition. Geochimica et Cosmochimica Acta, 72, 5304-
1195   5329.

1196

1197

1198

1199

1200

1201

1202

1203

1204

1205

1206

1207

1208

1209

1210

1211

1212

1213

1214

1215

1216

1217

1218

1219

1220 **Figure Captions:**

1221 **Fig. 1.** Geological map of the Singhbhum craton (modified after Saha (1994) and Upadhyay et
1222 al. (2014)) showing sample locations marked with solid circles. The inset map shows the
1223 different Indian cratons and other major geological units (Orogenic belts: 1. Mahakosal, 2.
1224 Satpura, 3. North Singhbhum, 4. Sakoli, 5. Dongargarh, 6. Eastern Ghats, 7. Pandyan;
1225 abbreviations: CGC = Chhotanagpur Gneiss Complex, SC = Singhbhum Craton, BC = Bastar
1226 Craton, EDC = Eastern Dharwar Craton, EDC = Western Dharwar Craton). Sample details are
1227 given in Table 1.

1228 **Fig. 2.** Classification diagram for the granitoids and volcanic rocks of the Singhbhum craton
1229 used in this study. (a) Granitoids classification based on their normative albite-anorthite-
1230 orthoclase composition (after Barker, 1979). Normative feldspar contents were calculated from
1231 whole rock major element analyses presented in Table 2. (b) Total Alkali Silica (TAS; SiO_2 wt.%
1232 on x-axis and Na_2O+K_2O wt.% on y-axis) rock type diagram for volcanic rocks (after Le Maitre et
1233 al. (1989)) based on whole rock major element composition presented in Table 2. For plotting,
1234 all the concentrations have been normalized to 100% after excluding loss on ignition (LOI).

1235 **Fig. 3.** Major-trace element variation diagrams based on whole rock major element composition
1236 presented in Table 2. All oxides are in wt.%; whereas, Sr, Nb, Ta, Yb, and Y are in parts per

million (ppm). For plotting, all oxide concentrations have been normalized to 100% after excluding loss on ignition (LOI). The marked high, medium, and low pressure fields are after Moyen (2011).

Fig. 4. Chondrite-normalized REE and primitive mantle normalized multi-element plots (Sun and McDonough, 1989) for the granitoids of the Singhbhum craton.

Fig. 5. Chondrite-normalized REE and primitive mantle normalized multi-element plots (Sun and McDonough, 1989) for the volcanic rocks of the Singhbhum craton.

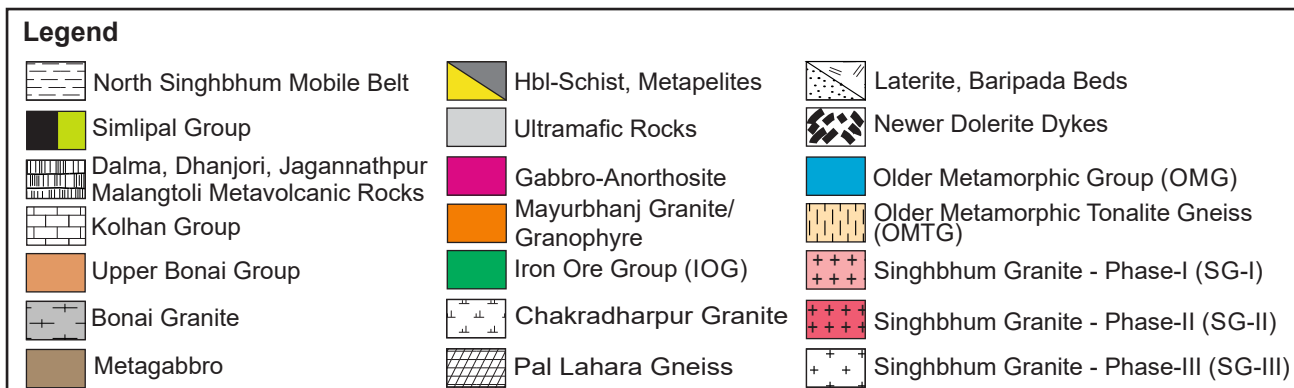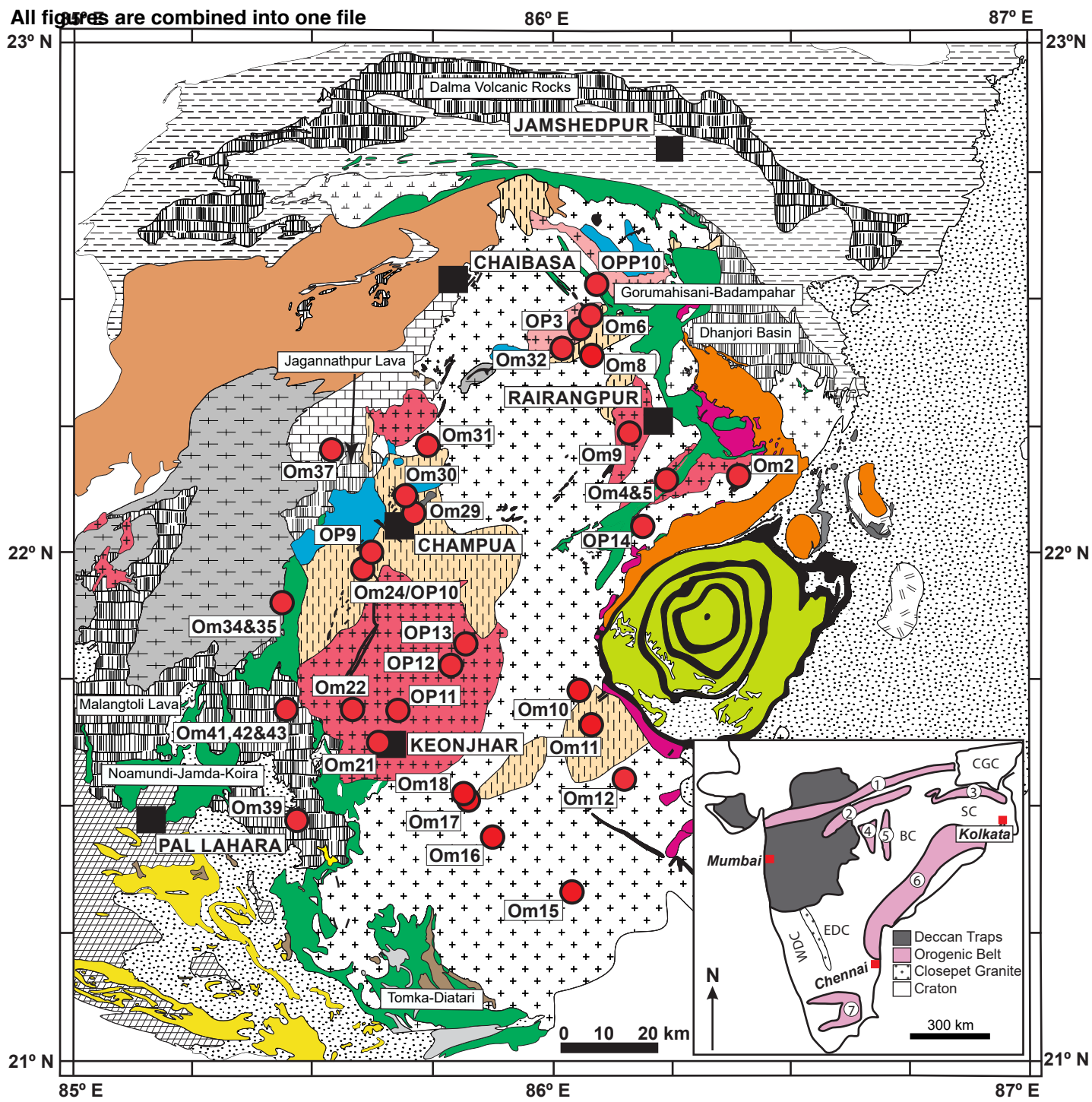**Fig. 6.** Common Pb isotope diagrams showing initial isotope compositions measured on leached K-feldspars separated from the granitoids of the Singhbhum craton (data presented in Table 3). Common Pb isotope data compilation for the Barberton greenstone belt and West Greenland are from Ulrych et al. (1967), Sinha and Tilton (1973), Kamber and Moorbath (1998), and Kamber et al. (2003). The curves correspond to the Pb-evolution curves Stacey and Kramers (1975) and, Kramers and Tolstikhin (1997). For details, see the text.

Fig. 7. Representative cathodoluminescence (CL) images of the zircon grains from the selected granitoids. The numbers marked on these images refer to their respective grain number. Dashed and solid circles (not to scale) show laser ablation spots for U-Pb and Hf isotope analyses, respectively. Analyses number (laser spots) for U-Pb and Hf isotope are named after the grain number (Appendix A2 and A4).

Fig. 8. Concordia diagrams showing the results of U-Pb analyses of the zircon grains from the selected granitoids (data in Appendix A2). Ellipses corresponding to 10% concordance (except inherited zircons) are color coded with light green.

Fig. 9. Whole rock Sm-Nd evolution diagrams for (a) older granitoids (except Om 12), (b) younger granitoids except (Om 11a), (c) East Singhbhum Volcanic Rocks (including komatiites), and (d) West Singhbhum Volcanic Rocks (except Om 37, Om 42, Om 43) of the Singhbhum craton. Ages given by the regression lines are not intended for strict geochronological purpose rather for petrogenetic context. (a), (b) Ages given by the Sm-Nd regression lines for the granitoids are in broad agreement (within uncertainties) with the zircon U-Pb ages. Whole rock Sm-Nd isotope data are presented in Table 4.

Fig. 10. Initial εNd versus age (Ga) and initial εHf versus age (Ga) plots. (a) Whole rock εNd_i vs. age plot for the granitoids of the Singhbhum craton from this study (data in presented in Table 4). (b) Zircon *(in-situ)* εHf_i vs. age plot for the selected granitoids from the Singhbhum craton (this study; Hf-isotope data for individual laser spots and mean for each sample presented in Appendix A4 and Table 5, respectively). The area shaded in yellow represents the scatter of individual analysis. (c) Whole rock εNd_i vs. age plot and, (d) Zircon εHf_i vs. age plot for some of the well-studied Hadean-early Archean rocks and zircons from the West Greenland, Acasta Gneisses, Kaapvaal craton (Southern Africa), and Yilgarn craton (West Australia) (data compilation from Bennett et al. (1993), Nutman et al. (1993), Bowring and Housh (1995), Iizuka et al. (2009), Kemp et al. (2009, 2010), Schoene et al. (2009), Nebel-Jacobsen et al. (2010), Zeh et al. (2011), Hoffmann et al. (2016), Reimink et al. (2016), Bauer et al. (2017) and, Fisher and Vervoort (2018)). Legends given in (a) are valid for (a) & (b) both. Abbreviations: DM = depleted mantle, CHUR = chondritic uniform reservoir; DM-1, DM-2, and DM-3 correspond to depleted mantle evolution model of Goldstein et al. (1984), Nägler and Kramers (1998), and DePaolo (1981) respectively. DM-Nd and DM-Hf refer to the depleted mantle Nd and Hf evolution trends proposed in this study.

Pandey et al. Fig. 1

Legend

- North Singhbhum Mobile Belt
- Simlipal Group
- Dalma, Dhanjori, Jagannathpur Malangtoli Metavolcanic Rocks
- Kolhan Group
- Upper Bonai Group
- Bonai Granite
- Metagabbro
- Hbl-Schist, Metapelites
- Ultramafic Rocks
- Gabbro-Anorthosite
- Mayurbhanj Granite/ Granophyre
- Iron Ore Group (IOG)
- Chakradharpur Granite
- Pal Lahara Gneiss
- Laterite, Baripada Beds
- Newer Dolerite Dykes
- Older Metamorphic Group (OMG)
- Older Metamorphic Tonalite Gneiss (OMTG)
- Singhbhum Granite - Phase-I (SG-I)
- Singhbhum Granite - Phase-II (SG-II)
- Singhbhum Granite - Phase-III (SG-III)

Pandey et al. Fig. 2

Pandey et al. Fig. 3
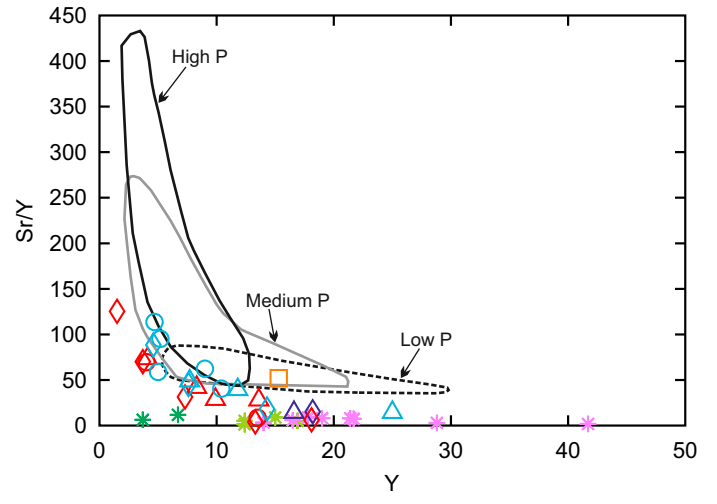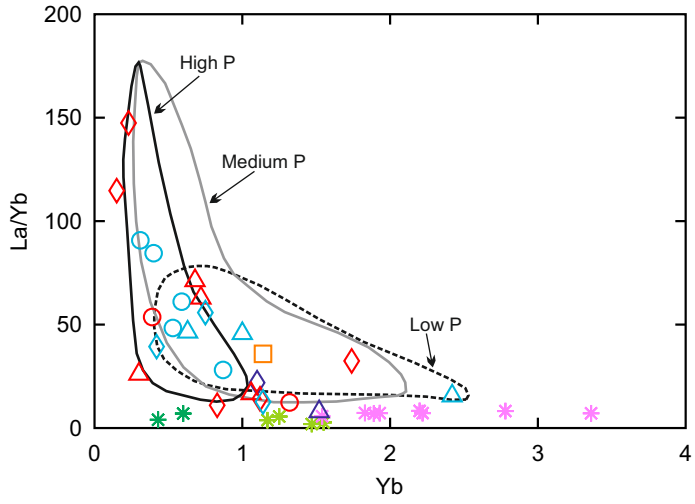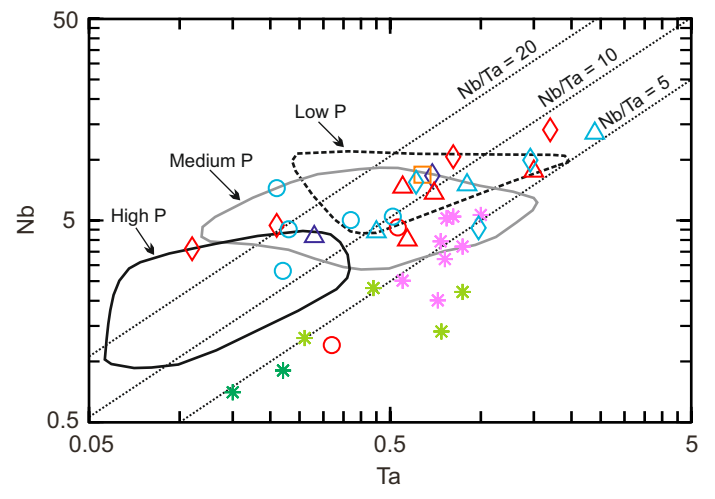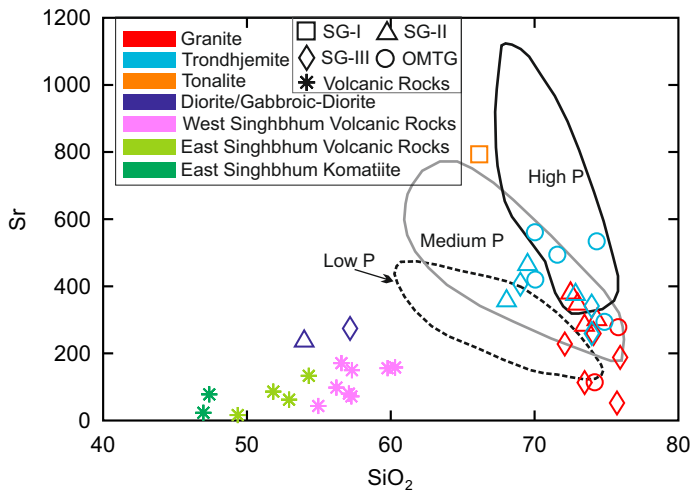
Pandey et al. Fig. 3 (continued)
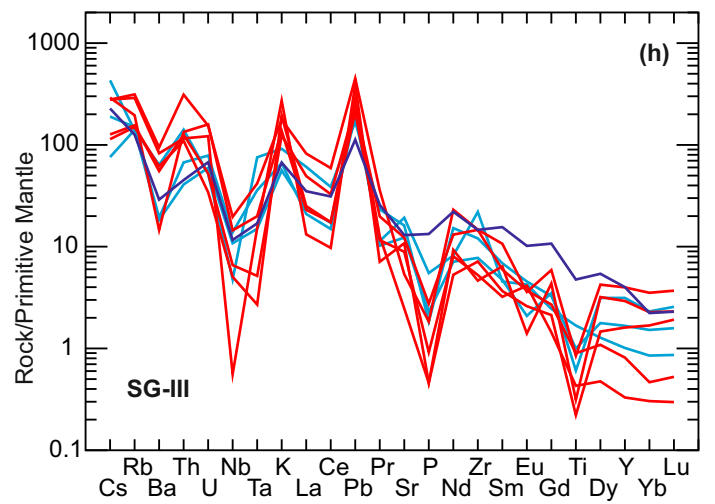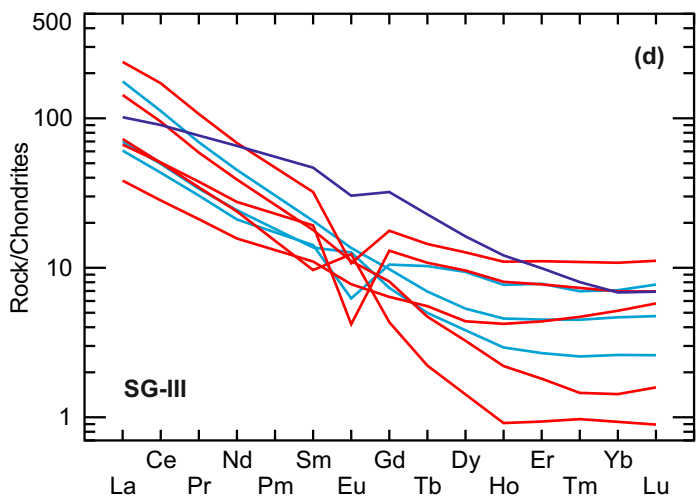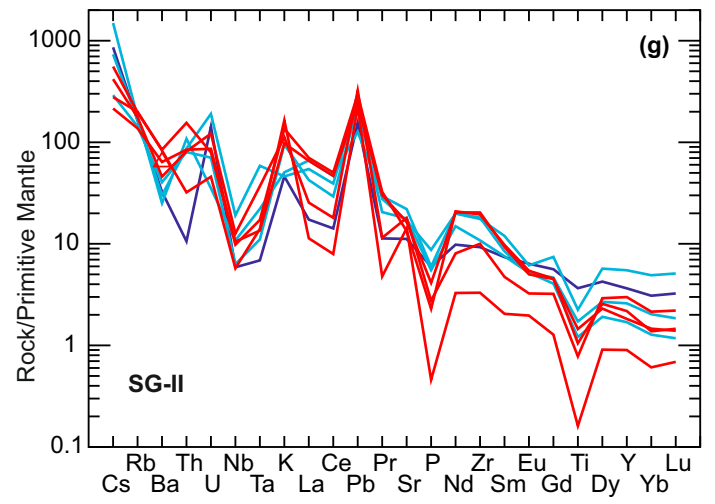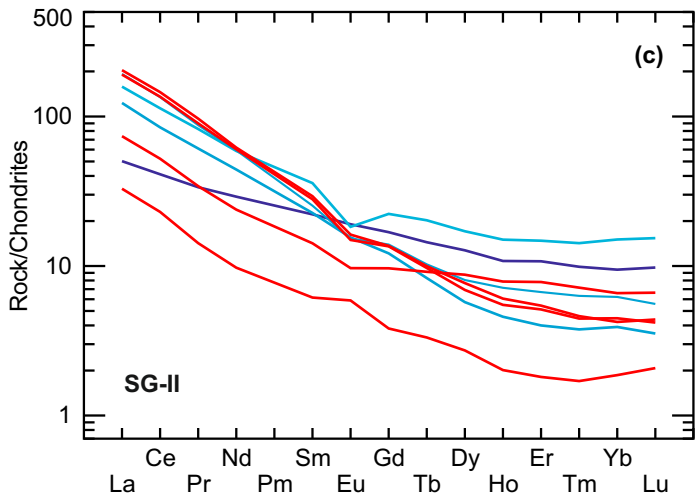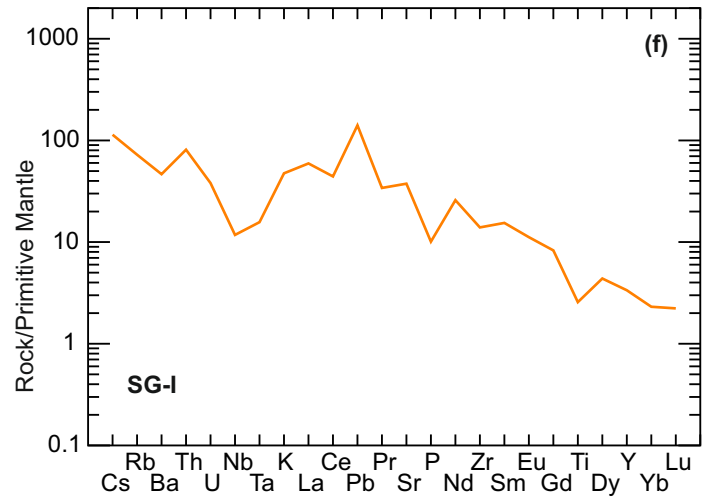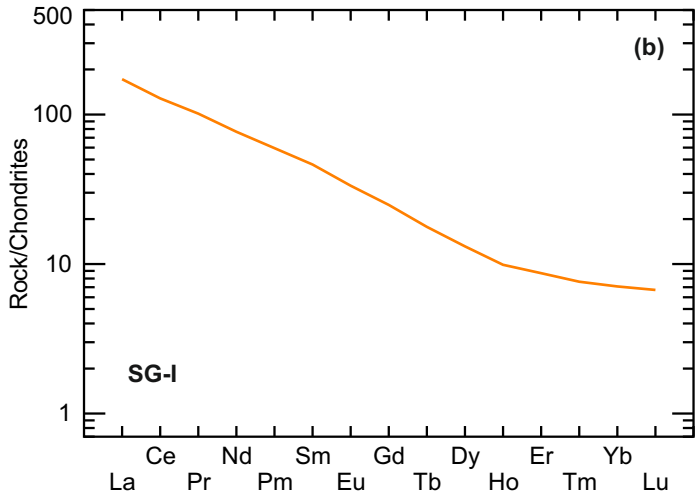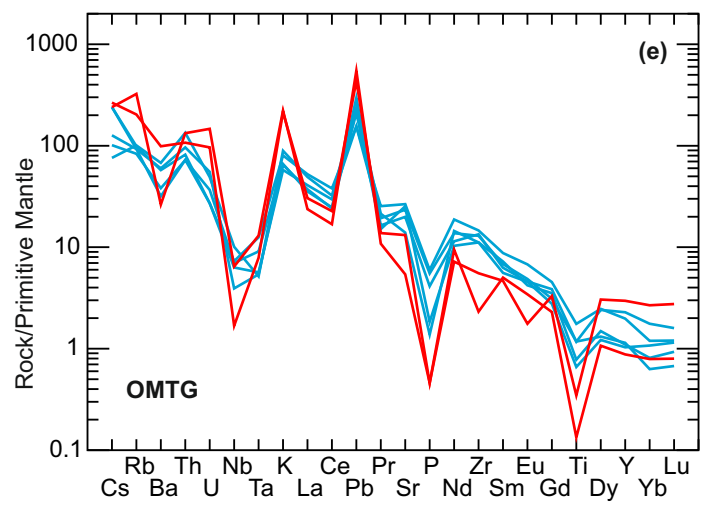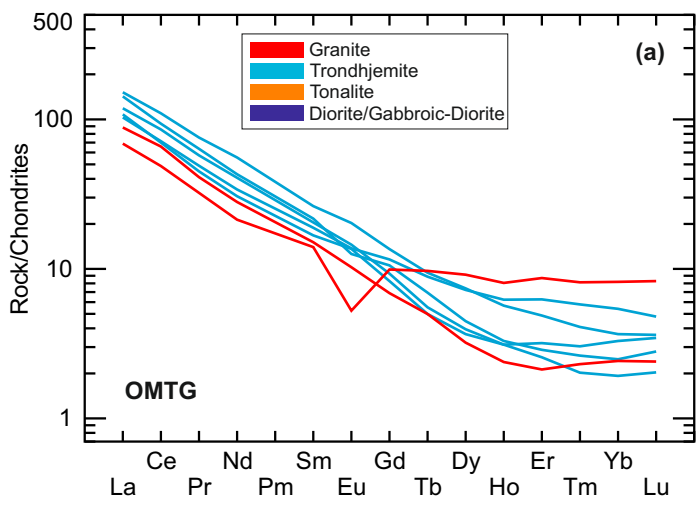
Pandey et al. Fig. 4
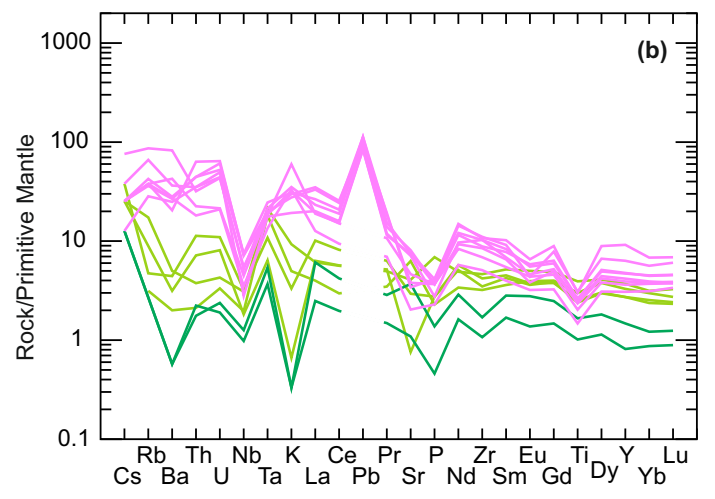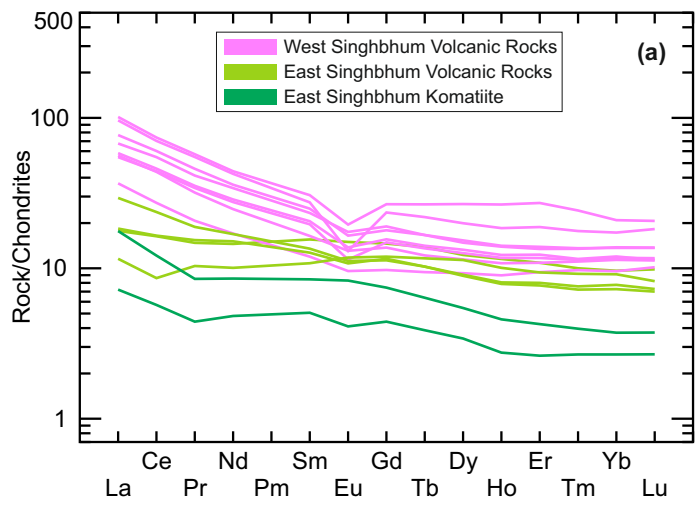
Pandey et al. Fig. 5
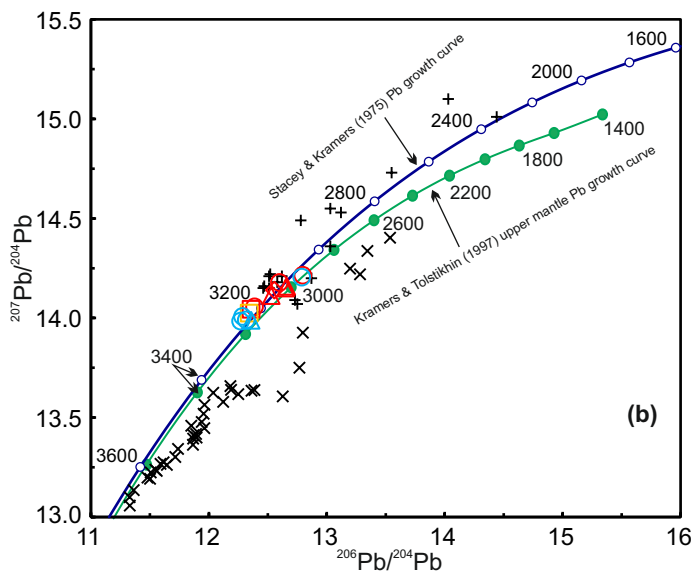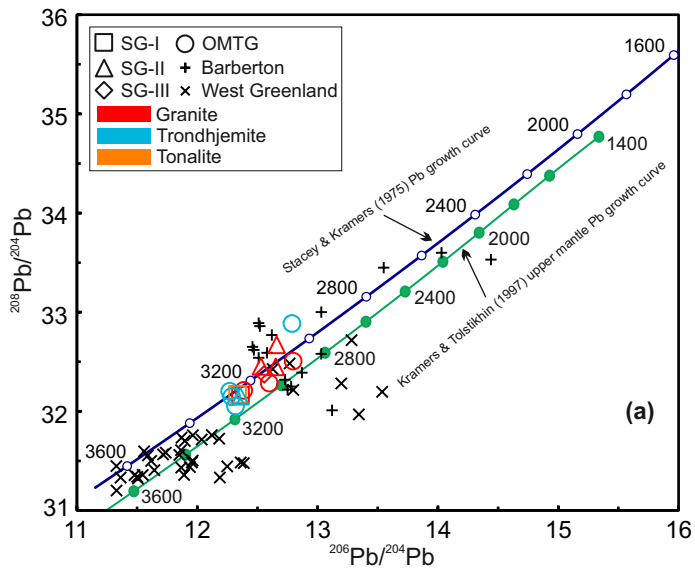
Pandey et al. Fig. 6
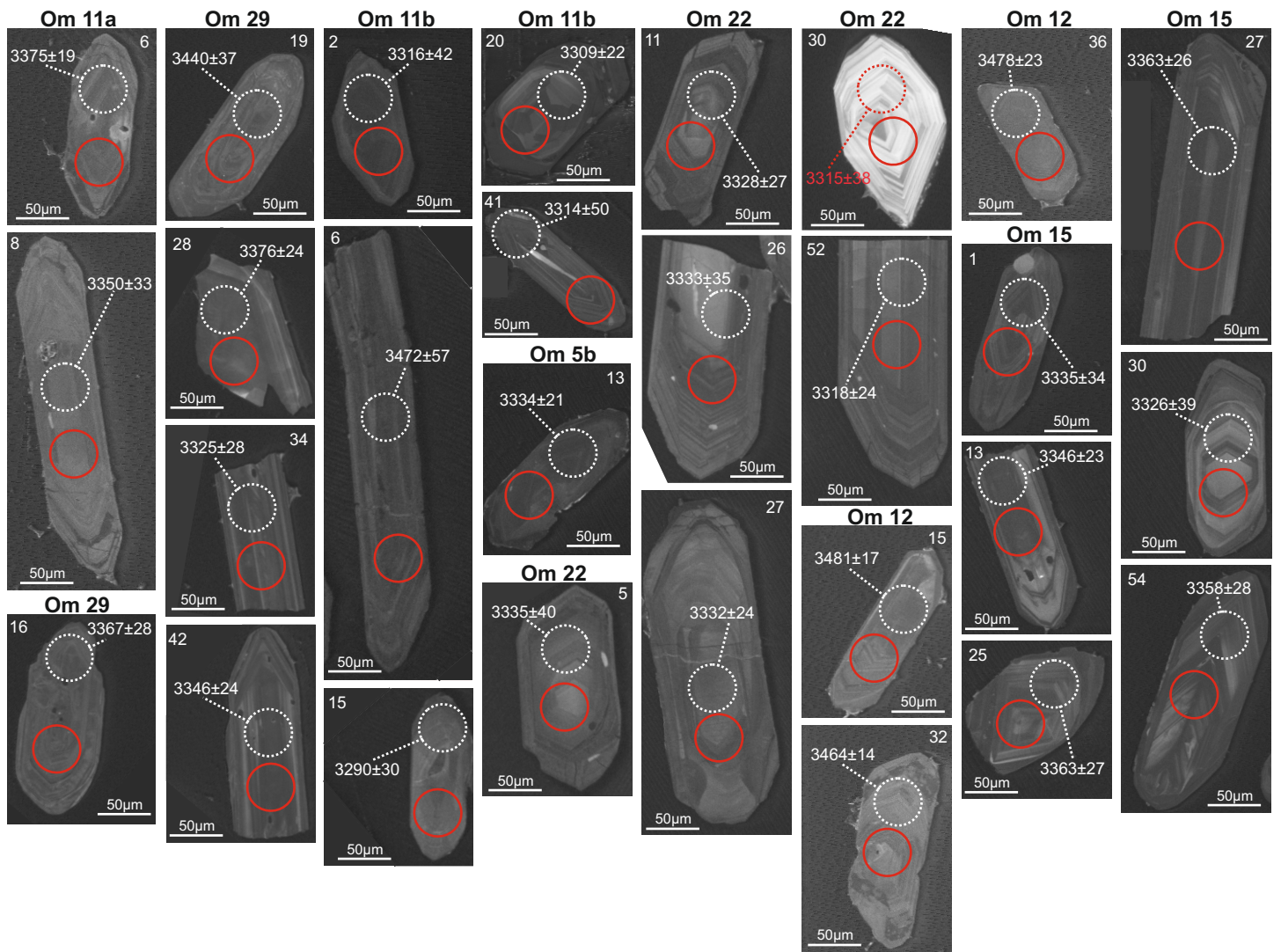
Pandey et al. Fig. 7
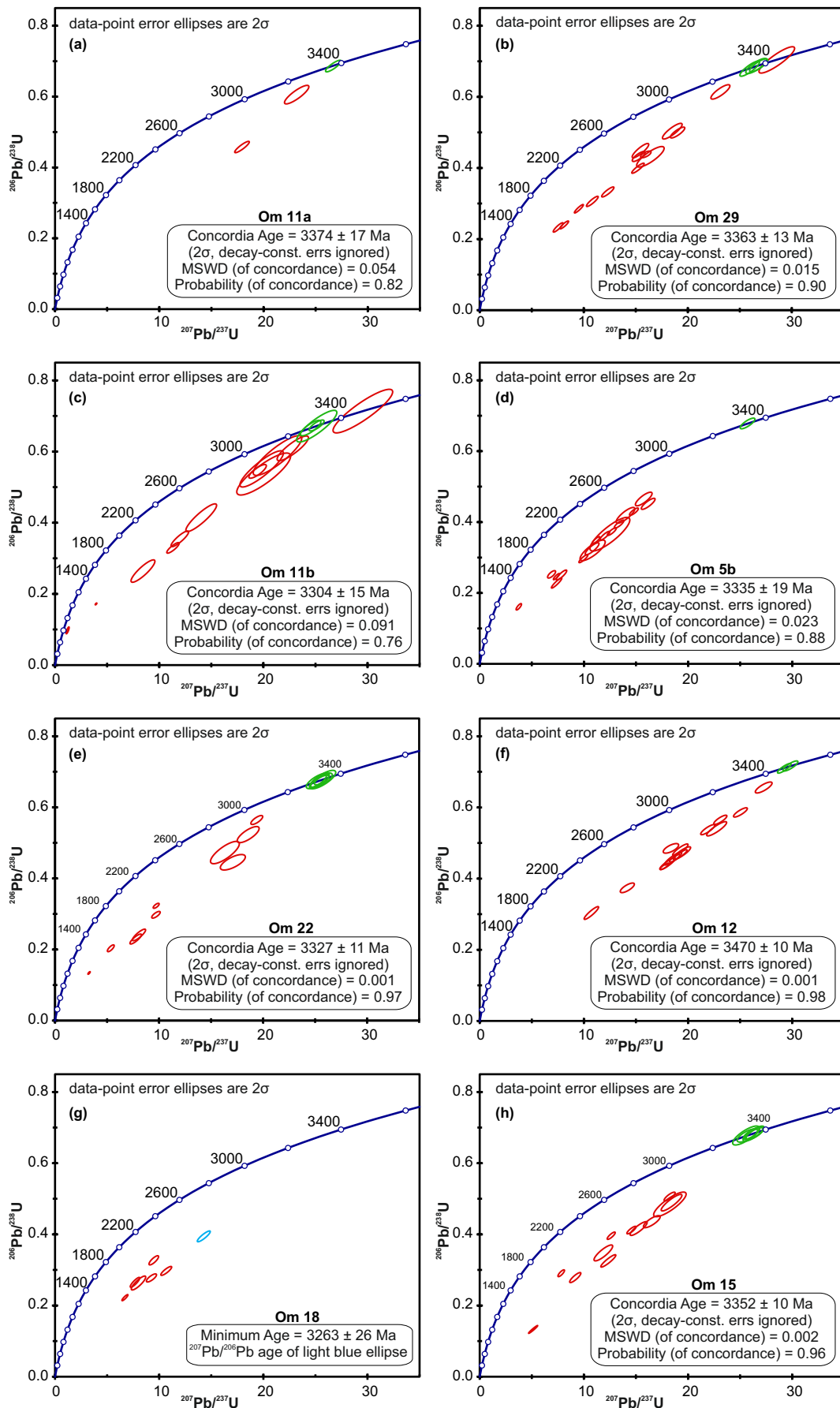
Pandey et al. Fig. 8
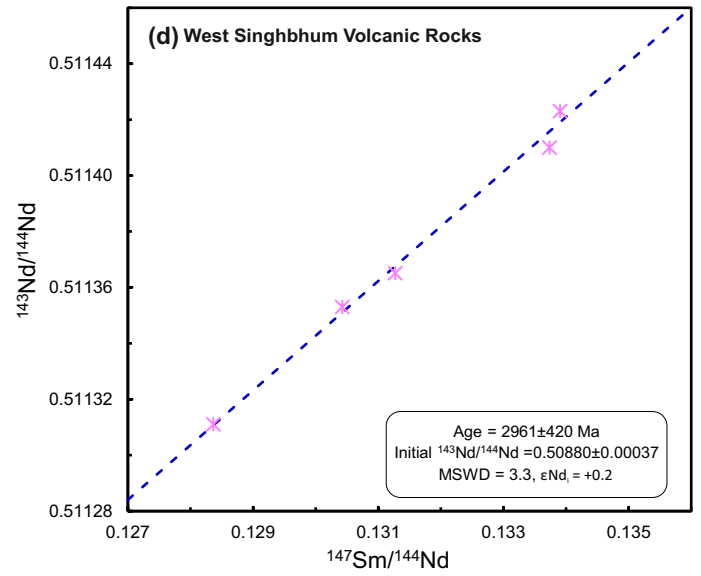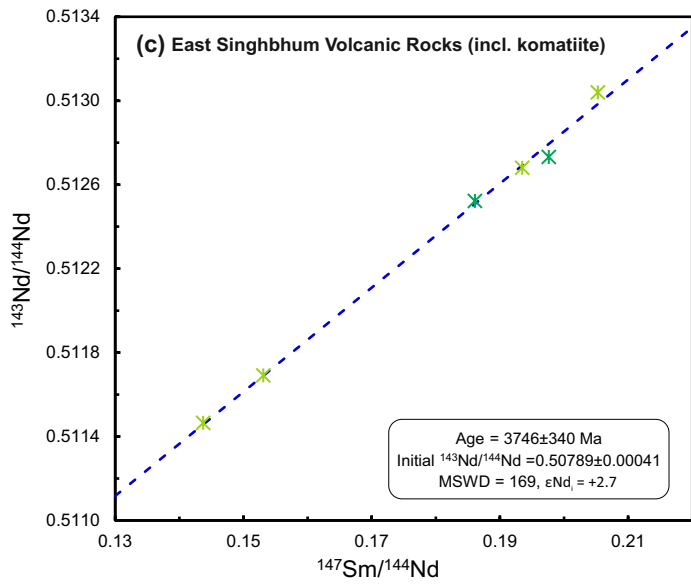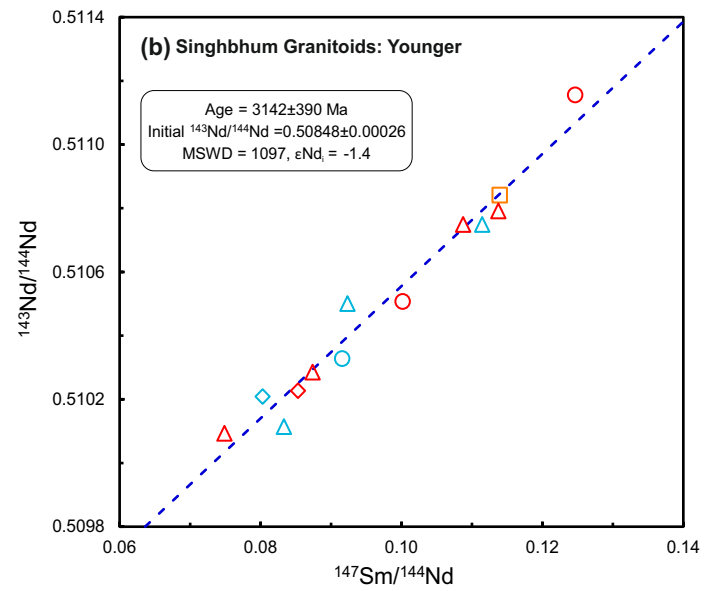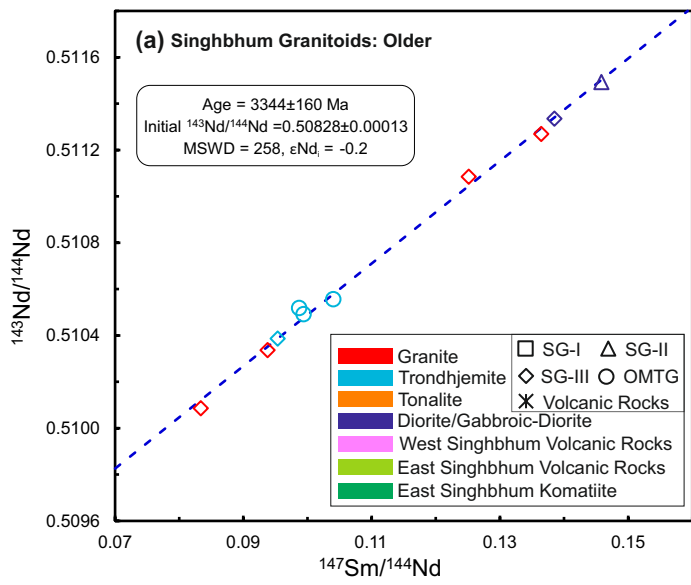
Pandey et al. Fig. 9
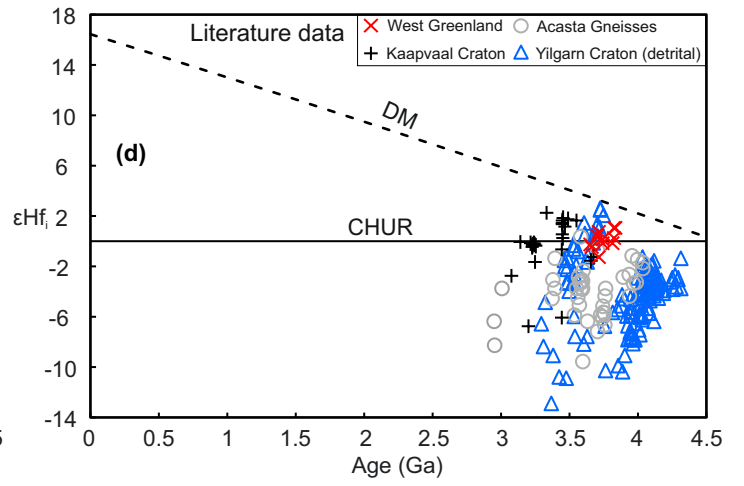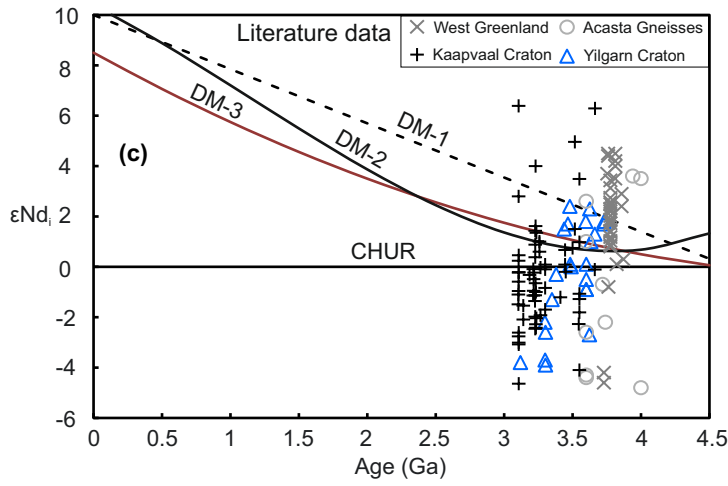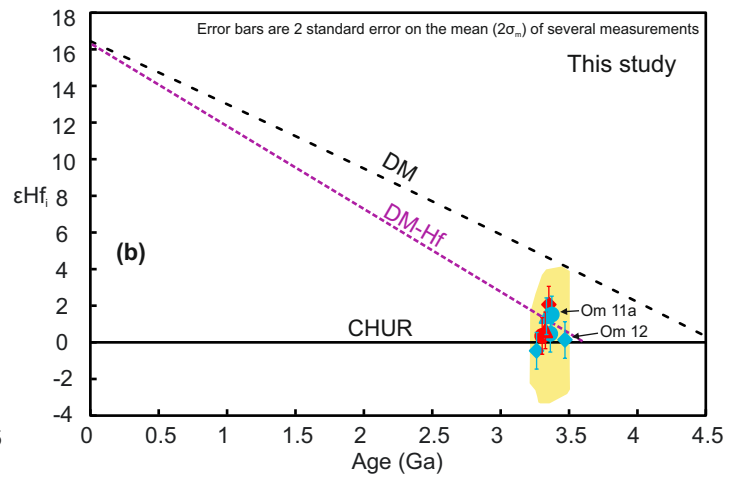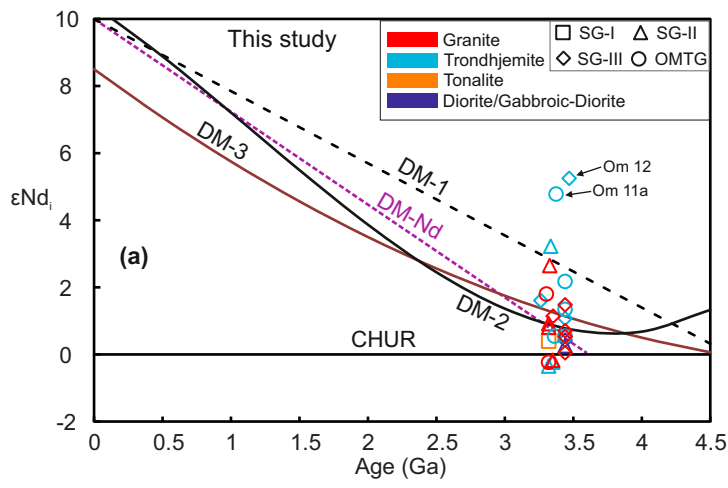
Pandey et al. Fig. 10

Table 1 Details of the samples and type of analyses performed on them.

Sample No.	Litho-Unit	Rock Type	Latitude (N)	Longitude (E)	Analysis Type
Om 8	OMTG	Trondhjemite	22° 23.452′	86° 04.871′	Kfs Common Pb; WR M-T, Rb-Sr, Sm-Nd
Om 11a	OMTG	Trondhjemite	21° 39.627′	86° 06.128′	WR M-T, Rb-Sr, Sm-Nd; Zircon U-Pb, Lu-Hf
Om 24/OP 10a	OMTG	Trondhjemite	21° 57.988′	85° 36.313′	Kfs Common Pb; WR M-T, Rb-Sr, Sm-Nd
Om 29	OMTG	Trondhjemite	22° 04.603′	85° 42.636′	Kfs Common Pb; WR M-T, Rb-Sr, Sm-Nd; Zircon U-Pb, Lu-Hf
Om 30b	OMTG	Trondhjemite	22° 06.667′	85° 41.607′	Kfs Common Pb; WR M-T, Rb-Sr, Sm-Nd
Om 11b	OMTG	Granite	21° 39.627′	86° 06.128′	WR M-T, Rb-Sr, Sm-Nd; Zircon U-Pb, Lu-Hf
Om 30a	OMTG	Granite	22° 06.667′	85° 41.607′	Kfs Common Pb; WR M-T, Rb-Sr, Sm-Nd
OP 9b	OMTG	Granite	22° 00.015′	85° 37.437′	Kfs Common Pb
OP 10b	OMTG	Granite	21° 57.988′	85° 36.313′	Kfs Common Pb
OP 3a	SG-I	Granite	22° 26.461′	86° 03.390′	Kfs Common Pb
OP 3b	SG-I	Tonalite	22° 26.461′	86° 03.390′	Kfs Common Pb; WR M-T, Rb-Sr, Sm-Nd
Om 32	SG-I	Tonalite	22° 24.210′	86° 01.123′	WR M-T, Rb-Sr, Sm-Nd
Om 2a	SG-II	Gabbroic-Diorite	22° 09.116′	86° 23.395′	WR M-T, Rb-Sr, Sm-Nd
Om 2b	SG-II	Trondhjemite	22° 09.116′	86° 23.395′	WR M-T, Rb-Sr, Sm-Nd
Om 5b	SG-II	Trondhjemite	22° 08.776′	86° 14.348′	WR M-T, Rb-Sr, Sm-Nd; Zircon U-Pb, Lu-Hf
Om 9c	SG-II	Trondhjemite	22° 14.191′	86° 09.613′	Kfs Common Pb
Om 9a	SG-II	Granite	22° 14.191′	86° 09.613′	WR M-T, Rb-Sr, Sm-Nd
Om 9b	SG-II	Granite	22° 14.191′	86° 09.613′	WR M-T, Rb-Sr, Sm-Nd
Om 21	SG-II	Granite	21° 37.489′	85° 38.265′	WR M-T, Rb-Sr, Sm-Nd
Om 22	SG-II	Granite	21° 41.375′	85° 35.038′	WR M-T, Rb-Sr, Sm-Nd; Zircon U-Pb, Lu-Hf
OP 11	SG-II	Granite	21° 41.290′	85° 40.685′	Kfs Common Pb
OP 12	SG-II	Granite	21° 46.657′	85° 47.249′	Kfs Common Pb
OP 13	SG-II	Granite	21° 49.045′	85° 48.874′	Kfs Common Pb
Om 10a	SG-III	Trondhjemite	21° 43.762′	86° 03.288′	WR M-T, Rb-Sr, Sm-Nd
Om 12	SG-III	Trondhjemite	21° 33.178′	86° 08.979′	WR M-T, Rb-Sr, Sm-Nd; Zircon U-Pb, Lu-Hf
Om 18	SG-III	Trondhjemite	21° 31.444′	85° 48.867′	WR M-T, Rb-Sr, Sm-Nd; Zircon U-Pb, Lu-Hf

Table 1 (continued) Details of the samples and type of analyses performed on them.

Sample No.	Litho-Unit	Rock Type	Latitude (N)	Longitude (E)	Analysis Type
Om 10c	SG-III	Granite	21° 43.762′	86° 03.288′	WR M-T, Rb-Sr, Sm-Nd
Om 15	SG-III	Granite	21° 19.886′	86° 02.373′	WR M-T, Rb-Sr, Sm-Nd; Zircon U-Pb, Lu-Hf
Om 16	SG-III	Granite	21° 26.436′	85° 52.343′	WR M-T, Rb-Sr, Sm-Nd
Om 17	SG-III	Granite	21° 30.668′	85° 49.464′	WR M-T, Rb-Sr, Sm-Nd
Om 31	SG-III	Granite	22° 12.605′	85° 44.338′	WR M-T, Rb-Sr, Sm-Nd
OP 14b	SG-III	Granite	22° 03.043′	86° 11.249′	Kfs Common Pb
Om 10b	SG-III	Diorite	21° 43.762′	86° 03.288′	WR M-T, Rb-Sr, Sm-Nd
Om 4a	EIOG	Basaltic Andesite	22° 08.776′	86° 14.066′	WR M-T, Rb-Sr, Sm-Nd
OPP 10e	EIOG	Basaltic Andesite	22° 32.220′	86° 05.420′	WR M-T, Rb-Sr, Sm-Nd
Om 4b	EIOG	Basalt	22° 08.776′	86° 14.066′	WR M-T, Rb-Sr, Sm-Nd
Om 6	EIOG	Basalt	22° 28.274′	86° 04.655′	WR M-T, Rb-Sr, Sm-Nd
OPP 10a	EIOG	Komatiite	22° 32.220′	86° 05.420′	WR M-T, Rb-Sr, Sm-Nd
OPP 10b	EIOG	Komatiite	22° 32.220′	86° 05.420′	WR M-T, Rb-Sr, Sm-Nd
Om 34	WIOG	Basaltic Andesite	21° 54.103′	85° 26.092′	WR M-T, Rb-Sr, Sm-Nd
Om 35a	WIOG	Andesite	21° 54.375′	85° 26.077′	WR M-T, Rb-Sr, Sm-Nd
Om 35b	WIOG	Andesite	21° 54.375′	85° 26.077′	WR M-T, Rb-Sr, Sm-Nd
Om 37	JL	Andesite	22° 12.173′	85° 32.372′	WR M-T, Rb-Sr, Sm-Nd
Om 39a	ML	Andesite	21° 28.449′	85° 27.931′	WR M-T, Rb-Sr, Sm-Nd
Om 41b	ML	Andesite	21° 41.517′	85° 26.606′	WR M-T, Rb-Sr, Sm-Nd
Om 42	ML	Basaltic Andesite	21° 41.612′	85° 26.749′	WR M-T, Rb-Sr, Sm-Nd
Om 43	ML	Basaltic Andesite	21° 41.493′	85° 27.361′	WR M-T, Rb-Sr, Sm-Nd

Abbreviations: OMTG = Older Metamorphic Tonalite Gneiss; SG-I, II, III = Singhbhum Granite Phase-I, II, III; EIOG = Eastern Iron Ore Group; WIOG = Western Iron Ore Group; JL = Jagannathpur Lava; ML = Malangtoli Lava; WR M-T = Whole rock major-trace element analyses; Kfs = K-feldspar.

Table 2 Major (wt.%) and trace (ppm) element composition of granitoids and volcanic rocks from the Singhbhum craton.

Analyte	Om 8	Om11a	Om24	Om 29	Om30b	Om11b	Om 30a	Om 32	Om 2a	Om 2b	Om 5b	Om 9c	Om 9a	Om 9b	Om 21	Om 22	Om 10a	Om 12	Om 18	Om 10c
SiO_2	69.21	74.34	72.74	71.03	69.58	72.78	74.38	64.02	52.81	67.24	72.52	69.06	73.82	72.27	72.72	72.29	68.31	72.30	72.50	72.05
Al_2O_3	15.98	14.00	14.59	15.00	15.11	13.87	13.25	15.85	11.69	16.01	14.23	16.04	14.11	15.22	14.01	14.32	16.24	14.11	14.43	15.31
$Fe_2O_{3(T)}$	3.00	1.72	1.69	2.47	3.32	1.00	0.68	4.64	11.45	4.32	2.54	3.65	1.22	1.88	2.10	2.52	3.21	2.12	1.62	0.59
MnO	0.044	0.026	0.021	0.036	0.042	0.017	0.007	0.058	0.190	0.079	0.043	0.057	0.016	0.041	0.030	0.028	0.045	0.037	0.025	0.011
MgO	0.78	0.29	0.32	0.80	0.87	0.12	0.07	1.67	8.16	1.19	0.55	0.74	0.07	0.31	0.25	0.46	1.02	0.41	0.35	0.06
CaO	2.56	1.44	1.75	2.76	2.92	0.53	0.55	4.19	10.33	3.19	2.28	2.43	0.95	1.61	1.09	1.92	2.61	1.64	1.53	0.53
Na_2O	5.19	4.77	4.79	5.26	4.93	3.12	2.73	4.60	2.03	5.14	4.39	5.71	4.24	4.93	4.61	4.39	5.69	5.15	4.69	3.18
K_2O	1.99	2.69	1.95	1.74	2.41	6.68	6.46	1.43	1.39	1.39	2.86	1.52	4.96	3.38	4.10	2.95	1.69	1.99	2.76	8.19
TiO_2	0.254	0.169	0.143	0.255	0.381	0.075	0.029	0.556	0.792	0.487	0.262	0.374	0.035	0.169	0.228	0.314	0.364	0.132	0.217	0.048
P_2O_5	0.09	0.03	0.04	0.12	0.13	0.01	0.01	0.22	0.13	0.19	0.12	0.13	0.01	0.06	0.05	0.09	0.12	0.05	0.04	0.01
LOI	1.02	0.49	1.06	0.82	0.63	0.44	0.66	1.44	1.38	1.02	0.83	0.58	0.27	0.32	0.99	0.96	0.71	0.78	0.87	0.50
Total	100.1	99.97	99.10	100.3	100.3	98.63	98.83	98.67	100.4	100.3	100.6	100.3	99.70	100.2	100.2	100.2	100.0	98.73	99.03	100.5
Sc	2	2	1	3	4	1	< 1	5	26	6	3	2	< 1	2	2	3	3	2	2	< 1
V	23	8	8	24	38	5	< 5	77	180	34	27	27	6	11	11	15	28	10	10	6
Cr	< 20	< 20	< 20	< 20	< 20	< 20	20	30	650	< 20	< 20	< 20	< 20	< 20	< 20	< 20	30	< 20	< 20	< 20
Co	5	2	2	5	7	2	2	11	56	8	4	6	< 1	2	2	3	6	2	< 1	2
Ni	< 20	< 20	< 20	< 20	< 20	< 20	< 20	20	340	< 20	< 20	< 20	< 20	< 20	< 20	< 20	< 20	< 20	< 20	< 20
Cu	< 10	< 10	< 10	< 10	< 10	< 10	< 10	< 10	160	10	10	< 10	< 10	< 10	< 10	10	< 10	< 10	< 10	10
Zn	50	< 30	< 30	50	50	< 30	< 30	50	90	60	40	50	< 30	< 30	40	50	50	30	40	< 30
Ga	19	15	17	20	20	16	11	19	15	21	18	21	17	19	18	18	20	20	19	21
Ge	1.0	0.7	0.7	0.8	0.9	1.1	1.1	0.9	1.8	1.1	0.9	0.8	0.9	0.8	0.9	0.8	0.8	0.8	0.8	1.2
Rb	53	64	59	59	63	206	129	46	104	105	91	112	127	112	125	87	88	95	89	184
Sr	420	294	534	494	561	114	278	793	236	356	375	464	300	379	283	346	406	259	341	228
Y	10.4	5.0	4.7	5.2	9.0	13.5	4.0	15.3	16.6	25.0	7.7	11.8	4.1	13.6	9.9	8.3	4.6	14.3	7.6	7.3
Zr	150	125	125	145	164	62	26	156	104	197	121	203	37	112	218	228	246	87	135	80
Nb	5.0	7.2	2.8	4.5	5.2	4.6	1.2	8.4	4.2	13.6	4.5	7.7	4.1	9.0	7.0	7.5	7.7	9.9	3.4	0.4
Cs	0.8	0.6	1.9	1.0	1.9	1.9	2.1	0.9	6.8	5.8	2.3	11.8	2.2	3.3	4.4	1.7	3.4	1.5	0.6	2.2
Ba	267	474	419	222	402	184	690	325	228	210	282	176	579	321	591	447	128	135	445	577
La	24.4	33.8	25.6	28.1	36.0	16.3	20.9	40.8	11.9	37.5	29.2	45.6	7.79	17.5	48.4	45.2	16.5	14.4	41.8	9.08
Ce	43.8	57.4	42.9	52.5	67.3	29.9	40.3	78.6	25.2	69.6	51.9	82.5	14.1	32.0	89.1	83.1	30.4	26.5	68.6	17.3
Pr	4.54	5.90	4.17	5.33	7.01	2.99	3.81	9.41	3.12	7.66	5.67	8.12	1.32	3.17	8.97	8.35	3.14	2.82	6.42	1.96
Nd	15.5	19.6	14.0	18.6	25.4	9.76	12.8	35.0	13.3	26.9	20.2	27.1	4.45	10.9	28.3	27.6	11.1	9.62	20.6	7.17
Sm	2.79	3.21	2.48	3.03	3.89	2.07	2.23	6.85	3.28	5.31	3.35	3.75	0.91	2.10	4.33	4.14	2.02	2.10	3.05	1.63
Eu	0.773	0.708	0.766	0.818	1.140	0.296	0.578	1.880	1.070	1.030	0.873	0.861	0.331	0.545	0.913	0.840	0.713	0.351	0.764	0.437
Gd	2.30	2.10	1.65	1.85	2.70	1.97	1.37	4.94	3.35	4.44	2.42	2.77	0.76	1.92	2.71	2.69	1.46	2.09	1.95	1.27
Tb	0.32	0.25	0.18	0.20	0.34	0.35	0.18	0.64	0.52	0.73	0.30	0.37	0.12	0.33	0.36	0.35	0.18	0.37	0.25	0.20
Dy	1.78	1.10	0.90	0.97	1.82	2.25	0.79	3.23	3.13	4.20	1.41	1.98	0.67	2.15	1.89	1.70	0.94	2.31	1.31	1.08
Ho	0.34	0.18	0.17	0.17	0.31	0.44	0.13	0.54	0.59	0.82	0.25	0.39	0.11	0.43	0.33	0.30	0.16	0.42	0.25	0.23
Er	1.0	0.46	0.51	0.41	0.78	1.39	0.34	1.39	1.72	2.36	0.64	1.07	0.29	1.25	0.87	0.82	0.43	1.25	0.72	0.70
Tm	0.143	0.065	0.075	0.050	0.101	0.201	0.057	0.188	0.244	0.351	0.093	0.156	0.042	0.177	0.114	0.110	0.063	0.172	0.111	0.116
Yb	0.87	0.40	0.53	0.31	0.59	1.32	0.39	1.14	1.52	2.42	0.63	1.00	0.30	1.06	0.68	0.72	0.42	1.14	0.75	0.83
Lu	0.118	0.069	0.085	0.050	0.089	0.204	0.059	0.165	0.240	0.378	0.087	0.137	0.051	0.163	0.108	0.103	0.064	0.190	0.117	0.142
Hf	2.9	3.1	2.8	3.1	3.1	1.7	0.9	3.5	2.2	3.9	2.6	4.1	1.2	2.4	4.1	4.7	4.6	2.3	3.1	2.2
Ta	0.37	0.21	0.22	0.23	0.51	0.53	0.32	0.64	0.28	2.39	0.45	0.90	0.57	1.50	0.70	0.55	0.61	1.46	3.07	0.62
Pb	21	17	15	11	11	39	31	10	11	19	16	9	16	23	21	17	14	19	12	28
Th	6.13	11.40	8.18	6.17	6.95	11.30	9.11	6.88	0.90	7.39	6.81	9.20	2.73	6.91	13.20	7.19	3.47	5.72	12.00	9.83
U	0.77	1.03	1.16	0.57	0.57	3.08	2.02	0.80	2.99	4.00	1.48	0.74	0.96	2.56	1.67	1.81	1.25	1.65	1.09	2.56
Nb/Ta	13.51	34.29	12.73	19.57	10.20	8.68	3.75	13.13	15.00	5.69	10.00	8.56	7.19	6.00	10.00	13.64	12.62	6.78	4.74	0.65
La/Yb	28.05	84.50	48.30	90.65	61.02	12.35	53.59	35.79	7.83	15.50	46.35	45.60	25.97	16.51	71.18	62.78	39.29	12.63	55.73	10.94
Sr/Y	40.38	58.80	113.62	95.00	62.33	8.44	69.50	51.83	14.22	14.24	48.70	39.32	73.17	27.87	28.59	41.69	88.26	18.11	44.87	31.23
Eu/Eu*	0.93	0.83	1.16	1.06	1.08	0.45	1.01	0.99	0.99	0.65	0.94	0.82	1.22	0.83	0.82	0.77	1.27	0.51	0.96	0.93

Table 2 (continued) Major (wt.%) and trace (ppm) element composition of granitoids and volcanic rocks from the Singhbhum craton.

Analyte	Om 15	Om 16	Om 17	Om 31	Om 10b	Om 4a	Om 4b	Om 6	OPP 10e	OPP 10a	OPP 10b	Om 34	Om 35a	Om 35b	Om 37	Om 39 a	Om 41b	Om 42	Om 43
SiO_2	73.23	75.88	74.96	72.56	55.97	50.45	46.38	50.40	53.44	41.74	43.36	54.93	54.99	55.72	54.17	58.60	57.36	53.74	51.75
Al_2O_3	13.98	13.09	13.42	14.28	13.51	6.53	5.95	7.95	8.32	1.09	2.15	11.26	12.38	13.18	11.98	13.01	11.54	11.55	10.00
$Fe_2O_3(T)$	1.89	1.26	1.36	1.73	8.60	12.97	12.98	12.54	12.65	9.91	12.69	10.28	10.99	10.03	10.09	9.40	8.75	8.47	8.57
MnO	0.024	0.011	0.025	0.028	0.098	0.209	0.185	0.204	0.212	0.193	0.189	0.158	0.165	0.171	0.153	0.132	0.135	0.141	0.159
MgO	0.27	0.10	0.09	0.22	6.95	14.60	20.13	12.22	9.34	34.95	27.37	7.83	7.29	6.79	8.20	6.15	7.95	10.78	12.91
CaO	1.52	0.80	0.74	0.78	7.01	9.44	8.89	12.66	14.43	1.69	6.51	9.81	8.44	6.79	7.21	7.39	6.72	7.50	8.67
Na_2O	4.10	2.94	4.31	3.75	3.28	1.70	0.13	1.23	0.43	0.03	0.11	2.14	1.58	3.99	2.57	1.85	1.98	2.75	1.58
K_2O	3.74	5.83	4.13	5.34	2.02	0.10	0.02	0.28	0.15	< 0.01	0.01	1.06	0.83	0.90	0.58	0.93	1.80	0.97	1.00
TiO_2	0.195	0.093	0.068	0.184	1.032	0.552	0.524	0.850	0.650	0.220	0.360	0.571	0.670	0.652	0.531	0.557	0.509	0.444	0.317
P_2O_5	0.06	0.02	< 0.01	0.04	0.29	0.06	0.06	0.15	0.05	< 0.01	0.03	0.08	0.08	0.09	0.06	0.09	0.08	0.08	0.05
LOI	0.52	0.37	0.74	0.69	1.40	2.31	4.35	1.22	1.09	10.14	6.59	1.89	3.47	2.44	3.27	2.54	2.54	3.53	3.74
Total	99.52	100.4	99.85	99.59	100.2	98.90	99.59	99.71	100.8	99.95	99.37	100.0	100.9	100.8	98.82	100.7	99.37	99.95	98.74
Sc	2	< 1	2	2	22	25	24	35	37	10	16	32	32	33	30	26	28	25	26
V	6	< 5	< 5	11	192	165	151	261	263	59	102	198	207	199	182	163	167	145	144
Cr	< 20	< 20	< 20	< 20	310	2070	2520	760	960	1240	1680	540	380	330	590	370	670	960	1380
Co	2	< 1	< 1	2	41	106	103	113	102	105	122	81	72	73	82	78	70	86	75
Ni	< 20	< 20	< 20	< 20	220	620	800	280	240	2070	1680	210	160	160	200	130	230	420	460
Cu	< 10	< 10	< 10	< 10	30	110	130	170	100	20	130	80	80	110	80	70	70	70	50
Zn	30	< 30	< 30	< 30	100	70	90	70	70	120	60	80	70	60	80	60	60	50	50
Ga	17	13	19	20	21	7	8	8	10	2	3	14	13	10	14	12	10	10	9
Ge	0.7	0.8	1.0	1.1	1.2	1.7	1.5	1.8	1.8	1.1	1.5	1.6	1.4	1.2	1.2	1.4	1.5	1.4	1.7
Rb	99	95	124	199	80	3	< 1	11	2	< 1	< 1	42	23	24	18	27	55	24	24
Sr	259	188	52	113	274	62	16	86	133	23	78	171	80	72	150	158	156	98	43
Y	3.7	1.5	13.3	18.1	18.2	12.4	12.4	16.9	15.0	3.7	6.7	21.4	28.8	41.7	19.0	21.7	17.8	16.5	14.0
Zr	164	59	52	165	164	47	39	52	36	12	19	99	124	120	115	115	95	77	57
Nb	4.7	3.6	10.3	14.0	8.3	2.3	1.3	2.2	1.4	0.7	0.9	3.7	5.2	5.1	2.0	5.3	3.9	3.2	2.5
Cs	1.0	0.9	2.3	2.2	1.8	0.3	0.2	0.2	< 0.1	0.1	0.1	0.3	0.2	0.2	0.1	0.2	0.6	0.2	0.2
Ba	387	430	102	662	203	31	22	35	14	4	4	254	187	143	174	196	576	298	190
La	33.9	17.2	15.8	56.4	24.1	6.95	4.35	4.20	2.74	1.71	4.19	16.0	22.8	24.0	13.8	18.2	13.0	13.3	8.70
Ce	58.2	30.9	31.0	105	55.3	14.5	10.1	10.0	5.27	3.50	7.45	33.6	43.1	45.4	28.2	36.9	27.1	26.8	16.7
Pr	5.47	3.20	3.49	9.90	7.12	1.75	1.43	1.37	0.96	0.41	0.79	3.84	5.10	5.32	3.28	4.26	3.17	2.96	1.92
Nd	17.8	10.9	12.6	31.2	29.9	7.71	6.91	6.64	4.60	2.20	3.90	15.6	19.4	20.2	13.1	16.4	12.6	11.3	7.79
Sm	2.65	1.43	2.84	4.75	6.92	2.00	1.88	2.30	1.60	0.75	1.25	3.45	4.06	4.53	3.04	3.69	2.90	2.43	1.77
Eu	0.624	0.693	0.236	0.604	1.710	0.630	0.607	0.842	0.663	0.231	0.467	0.981	0.734	1.100	0.775	0.928	0.643	0.735	0.540
Gd	1.61	0.86	2.59	3.52	6.38	2.25	2.30	2.90	2.38	0.88	1.48	3.78	4.67	5.31	3.10	3.56	2.96	2.73	1.94
Tb	0.17	0.08	0.39	0.52	0.82	0.37	0.37	0.50	0.42	0.14	0.23	0.60	0.79	0.96	0.51	0.60	0.49	0.44	0.34
Dy	0.80	0.35	2.36	3.12	3.99	2.23	2.19	3.02	2.79	0.84	1.34	3.64	4.90	6.58	3.27	3.77	3.10	2.82	2.28
Ho	0.12	0.05	0.44	0.60	0.66	0.44	0.43	0.63	0.55	0.15	0.25	0.76	1.01	1.45	0.67	0.77	0.64	0.59	0.49
Er	0.29	0.15	1.24	1.77	1.59	1.28	1.23	1.74	1.50	0.42	0.68	2.15	3.01	4.35	1.97	2.22	1.87	1.74	1.51
Tm	0.036	0.024	0.181	0.270	0.198	0.187	0.178	0.247	0.227	0.066	0.098	0.333	0.437	0.598	0.285	0.336	0.281	0.274	0.240
Yb	0.23	0.15	1.12	1.74	1.10	1.25	1.17	1.55	1.47	0.43	0.60	2.22	2.78	3.36	1.93	2.20	1.89	1.83	1.54
Lu	0.039	0.022	0.171	0.274	0.170	0.179	0.172	0.242	0.202	0.066	0.092	0.338	0.448	0.508	0.280	0.336	0.287	0.277	0.250
Hf	3.3	1.6	1.8	4.1	3.7	1.1	1.0	1.3	0.9	0.3	0.5	2.2	2.6	2.6	2.8	2.6	2.2	1.7	1.4
Ta	0.21	0.11	0.81	1.70	0.69	0.44	0.26	0.87	0.74	0.15	0.22	0.87	0.81	0.77	0.72	1.00	0.74	0.76	0.55
Pb	17	15	20	32	8	< 5	< 5	< 5	< 5	< 5	< 5	7	8	7	6	8	6	< 5	< 5
Th	10.70	9.33	11.40	26.50	3.84	0.96	0.61	0.32	0.18	0.19	0.15	2.98	3.78	5.39	2.99	3.78	2.71	1.91	1.54
U	1.10	0.72	3.34	3.24	1.42	0.23	0.17	0.09	0.07	0.04	0.05	0.93	1.10	1.35	1.04	1.28	0.91	0.45	0.44
Nb/Ta	22.38	32.73	12.72	8.24	12.03	5.23	5.00	2.53	1.89	4.67	4.09	4.25	6.42	6.62	2.78	5.30	5.27	4.21	4.55
La/Yb	147.39	114.67	14.11	32.41	21.91	5.56	3.72	2.71	1.86	3.98	6.98	7.21	8.20	7.14	7.15	8.27	6.88	7.27	5.65
Sr/Y	70.00	125.33	3.91	6.24	15.05	5.00	1.29	5.09	8.87	6.22	11.64	7.99	2.78	1.73	7.89	7.28	8.76	5.94	3.07
Eu/Eu*	0.93	1.91	0.27	0.45	0.79	0.91	0.89	1.00	1.04	0.87	1.05	0.83	0.52	0.69	0.77	0.78	0.67	0.87	0.89

LOI = loss on ignition; Eu/Eu* = $(Eu)_N/\{(Sm)_N \times (Gd)_N\}^{1/2}$; $(Eu)_N$, $(Sm)_N$, and $(Gd)_N$, are normalized to chondrite (Sun and McDonough, 1989).

Table 3 Common Pb isotope data from leached K-feldspars of granitoids of the Singhbhum craton.

Sample No.	$^{206}Pb/^{204}Pb$	1 se	$^{207}Pb/^{204}Pb$	1 se	$^{208}Pb/^{204}Pb$	1 se
Om 8	12.3192	0.0018	13.9899	0.0020	32.051	0.005
Om 30b	12.2869	0.0008	14.0066	0.0012	32.146	0.004
Om 29	12.2705	0.0029	13.9837	0.0033	32.200	0.008
Om 24/OP 10a	12.7887	0.0009	14.2047	0.0011	32.884	0.003
Om 30a	12.3872	0.0008	14.0555	0.0014	32.210	0.004
OP 9b	12.5983	0.0009	14.1776	0.0013	32.285	0.004
OP 10b	12.7974	0.0045	14.2142	0.0050	32.505	0.010
OP 3a	12.3594	0.0009	14.0432	0.0013	32.165	0.004
OP 3b	12.3361	0.0008	14.0254	0.0013	32.172	0.004
Om 9c	12.3586	0.0007	13.9879	0.0008	32.153	0.002
OP 11	12.6599	0.0009	14.1587	0.0012	32.672	0.003
OP 12	12.5290	0.0006	14.1126	0.0008	32.453	0.003
OP 13	12.6519	0.0007	14.1503	0.0010	32.449	0.003
OP 14b	12.5557	0.0006	14.1398	0.0008	32.372	0.002

Pb isotope ratios are corrected for isobaric interference and mass bias. se = standard error

Table 4 Sm-Nd isotope data for granitoids and volcanic rocks of the Singhbhum craton.

Sample No.	Age (Ma)	Sm (ppm)	Nd (ppm)	$^{147}Sm/^{144}Nd$	$^{143}Nd/^{144}Nd$	2se	$(^{143}Nd/^{144}Nd)_i$	εNd_i
Om 8	3440	2.890	16.79	0.1040	0.510557	0.000003	0.508190	+0.5
Om 11a	**3374**	4.289	29.92	0.0866	0.510425	0.000004	0.508492	+4.8
Om 24/OP 10a	3440	2.446	14.98	0.0986	0.510519	0.000003	0.508273	+2.2
Om 29	**3363**	2.901	19.14	0.0916	0.510328	0.000004	0.508292	+0.5
Om 30b	3440	4.844	29.45	0.0994	0.510492	0.000004	0.508231	+1.3
Om 11b	**3304**	2.432	11.79	0.1246	0.511156	0.000004	0.508433	+1.8
Om 30a	3320	2.209	13.33	0.1002	0.510507	0.000004	0.508308	-0.2
Om 32	3320	6.926	36.73	0.1139	0.510842	0.000003	0.508340	+0.4
Om 2a	3440	3.722	15.43	0.1458	0.511494	0.000003	0.508175	+0.3
Om 2b	3320	6.829	37.03	0.1115	0.510749	0.000002	0.508303	-0.3
Om 5b	**3335**	3.876	25.37	0.0923	0.510501	0.000002	0.508465	+3.2
Om 9c	3350	4.503	32.66	0.0833	0.510115	0.000003	0.508269	-0.2
Om 9a	3350	0.7141	3.794	0.1137	0.510792	0.000005	0.508272	-0.2
Om 9b	3320	2.598	14.43	0.1087	0.510749	0.000008	0.508362	+0.8
Om 21	3320	4.027	27.84	0.0874	0.510285	0.000006	0.508367	+0.9
Om 22	**3327**	6.266	50.55	0.0749	0.510093	0.000007	0.508446	+2.6
Om 10a	3440	2.385	15.11	0.0953	0.510387	0.000003	0.508217	+1.1
Om 12	**3470**	3.030	15.63	0.1172	0.511079	0.000004	0.508390	+5.2
Om 18	**3263**	3.562	26.80	0.0803	0.510209	0.000006	0.508477	+1.6
Om 10c	3440	1.502	7.251	0.1251	0.511085	0.000004	0.508238	+1.5
Om 15	**3352**	3.234	22.90	0.0853	0.510227	0.000005	0.508336	+1.1
Om 16	3440	1.258	9.119	0.0834	0.510086	0.000004	0.508190	+0.5
Om 17	3440	3.422	15.16	0.1364	0.511270	0.000005	0.508165	+0.1
Om 31	3440	42.77	275.3	0.0939	0.510334	0.000002	0.508199	+0.7
Om 10b	3440	7.084	30.91	0.1385	0.511336	0.000003	0.508184	+0.4
Om 4a	*3746*	2.019	7.972	0.1531	0.511691	0.000002	0.507894	+2.6
Om 4b	*3746*	1.864	7.840	0.1437	0.511465	0.000063	0.507900	+2.8
Om 6	*3746*	2.351	7.346	0.1935	0.512680	0.000002	0.507881	+2.4
OPP 10e	*3746*	1.623	4.780	0.2053	0.513039	0.000003	0.507947	+3.7
OPP 10a	*3746*	0.6987	2.137	0.1976	0.512732	0.000005	0.507830	+1.4
OPP 10b	*3746*	1.242	4.034	0.1861	0.512522	0.000005	0.507906	+2.9
Om 34	*2961*	3.404	15.36	0.1339	0.511423	0.000002	0.508805	+0.3
Om 35a	*2961*	3.883	17.99	0.1304	0.511353	0.000003	0.508803	+0.2
Om 35b	*2961*	3.712	17.09	0.1313	0.511365	0.000003	0.508798	+0.1
Om 37	*2961*	3.017	13.62	0.1339	0.511394	0.000003	0.508776	-0.3
Om 39a	*2961*	3.711	17.47	0.1284	0.511311	0.000003	0.508801	+0.2
Om 41b	*2961*	2.884	13.03	0.1337	0.511410	0.000007	0.508795	+0.1
Om 42	*2961*	2.443	11.58	0.1275	0.511254	0.000003	0.508761	-0.6
Om 43	*2961*	1.684	7.524	0.1353	0.511393	0.000002	0.508748	-0.9

se = standard error on the mean; i = initial; Parameters used for initial $^{143}Nd/^{144}Nd$ and εNd calculation are as follows:
$(^{143}Nd/^{144}Nd)_{CHUR t_0}$ = 0.512638; $(^{147}Sm/^{144}Nd)_{CHUR t_0}$ = 0.1967; λ_{147Sm} = 6.54 x 10^{-12} year^{-1}
CHUR = chondritic uniform reservoir; t_0 = present day; errors on Sm, Nd concentration and $^{147}Sm/^{144}Nd$ are ~0.1%; error on εNd_i is ~1ε.
Ages in bold and italics are U-Pb zircon ages and Sm-Nd whole rock regression line ages respectively from this study and rest are from Upadhyay et al. (2014). The initial $^{143}Nd/^{144}Nd$ and εNd for the volcanic rocks (Om 4a to Om 43) are calculated and reported here based on ages obtained from the Sm-Nd regression lines with high MSWD, hence are not robust and not used for crustal evolution interpretation.

Table 5 Mean initial εHf_i zircon LA-MC-ICP-MS data for selected granitoids of the Singhbhum craton (detailed data presented in Appendix A3).

Sample No.	Litho-unit	Rock-type	Assigned age (Ma)	±2σ	εHf_i (mean)	±2σ$_m$	Number of analyses (n)	εNd_i (whole rock)
Om 11a	OMTG	Trondhjemite	3374	17	+1.5	1.0	6	+4.8
Om 29	OMTG	Trondhjemite	3363	13	+0.6	1.2	9	+0.5
Om 11b	OMTG	Granite	3304	15	+0.1	0.9	9	+1.8
Om 5b	SG II	Trondhjemite	3335	19	+1.4	0.4	10	+3.2
Om 22	SG II	Granite	3327	11	+0.7	0.9	11	+2.6
Om 12	SG III	Trondhjemite	3470	10	+0.1	1.1	11	+5.2
Om 18	SG III	Trondhjemite	3263	26	-0.5	0.8	9	+1.6
Om 15	SG III	Granite	3352	15	+2.1	0.6	14	+1.1

σ_m is standard error on the mean. Assigned ages are U-Pb LA-ICP-MS zircon ages from this study.

All supplementary appendices are merged into a single file

[Click here to download Background dataset for online publication only: Appendices combined_Pandey et al..pdf](#)